

## Contents

<b>I. Introduction</b>	4
<b>II. Classical and Quantum Electrodynamics of Polaritonic Vortices</b>	6
<b>III. Tunable Selection Rules</b>	9
<b>IV. Discussion</b>	11
<b>V. Conclusion</b>	14
<b>References</b>	21
<b>VI. Introduction to Supplementary Material</b>	28
<b>VII. Appendix 1: Construction of Classical Polaritonic Vortex Modes in (An)isotropic Dielectrics</b>	28
A. General Construction	28
B. Energy and Orthogonality of Vortex Modes	30
1. Angular Momentum Representation of Displaced Vortices	31
C. Quasi-Electrostatic Limit: Scalar Potential Formalism	31
<b>VIII. Appendix 2: Construction of Quantum Fields for Polaritonic Vortices in the Angular Momentum Basis</b>	33
A. Field Operators	33
1. Vector Potential in the $\phi = 0$ Gauge	34
2. Scalar Potential in the Coulomb Gauge: $\nabla \cdot \mathbf{A} = 0$	35
3. $\xi_q$ for Different Materials	35
<b>IX. Appendix 3: Angular Momentum and Light-Matter Interactions</b>	37
A. First-Order Processes	37
1. Long-Wavelength Approximation	39
2. Absorption rates of $m_{vortex} = 5$ SP(h)P mode with starting state (5,0,0)	40
B. Second-Order Processes	41

1. Spontaneous Emission in the Angular Momentum Basis	41
2. Absorption of Two-Vortices	43
<b>References</b>	43

# Shaping Polaritons to Reshape Selection Rules

Francisco Machado<sup>\*1</sup>, Nicholas Rivera<sup>\*1</sup>, Hrvoje Buljan<sup>2</sup>, Marin Soljačić<sup>1</sup>, Ido Kaminer<sup>1</sup>

<sup>1</sup>*Department of Physics, Massachusetts Institute of Technology, Cambridge, MA 02139, USA*

<sup>2</sup>*Department of Physics, University of Zagreb, Zagreb 10000, Croatia.*

## Abstract

The discovery of orbital angular momentum (OAM) in photonics established a new degree of freedom by which to control not only the flow of light but also its interaction with matter. Here, we show that it is possible to use OAM carrying plasmon and phonon polaritons to engineer new selection rules in electronic systems, such as atoms, molecules, and artificial atoms (e.g. quantum dots), thus introducing a new degree of freedom for controlling once-forbidden transitions. This arises by granting OAM to polaritons whose short wavelength enables access to conventionally forbidden electronic transitions. We show that these selection rules can be robust to displacements of the electronic system relative to the vortex center. We also show that the position of the absorber provides a surprisingly rich parameter for controlling which absorption processes dominate over others. The same effect can be achieved by altering the plasmonic properties of a material, for example by tuning the carrier density in graphene. Our findings are best suited to vortex modes that can be created in graphene, monolayer conductors, ultrathin metallic films, thin films of hBN and other polar dielectrics.

## I. INTRODUCTION

The discovery of light-sustaining orbital angular momentum (OAM) [1] has brought forth a new degree of freedom for the photon, enabling a wave of novel applications of light. Examples of such applications include angular manipulation of objects [2], angular velocity measurement [3], higher bandwidths communication using novel multiplexing techniques [4, 5] (already with on-chip implementations [6]), new quantum information systems [7], quantum memory [8] and sources of entangled light [9], which are beneficial to quantum cryptography implementations [10, 11]. The same concept of granting light OAM by shaping its phase profile has even been extended to the Schrödinger wave function for free electrons with direct application to electron beam physics [12–16]. Analogous to electron beam physics, the concept of OAM can be applied directly at the single photon level by shaping the phase profile of electromagnetic modes. This remarkable fact enables a single photon to carry angular momentum beyond its intrinsic spin value of  $\hbar$ , expanding the realm of possible applications of light. A crucial consequence that immediately follows is the possibility of shaping the landscape of electronic transitions in atom-like systems.

Unfortunately, such novel phenomena are not expected to be experimentally accessible because “the effective cross section of the atom is extremely small; so the helical phase front is locally indistinguishable from an inclined plane wave” [17]. This is true when the atom is away from the center of the OAM carrying vortex and is thus no longer exposed to the rapid phase variation at the origin. Moreover, even when the atom is at the vortex center, due to the mismatch between the spatial scale of the electromagnetic field variations and the size of the electronic orbitals, the forbidden transitions to which this idea applies [18] would be still far too slow to be clearly observable. Such a prediction has been corroborated in several theoretical studies [19–22]. That said, there can exist rare cases where quadrupole transitions can be interfaced with OAM [23], but it is still quite challenging in these scenarios. Because observing the quadrupole transition is already challenging, efforts to observe the infinitely many other higher-order multipole transitions (and other classes of forbidden transitions) would seem hopeless. Therefore, new approaches will be necessary to use OAM to control and explore forbidden electronic transitions in a wide variety of atoms, molecules, and other electronic systems. In these approaches it will be absolutely necessary to bridge the disparate length scales of the electronic system and photon.

Recent discoveries in the blossoming field of surface polaritons, ranging from surface plasmon

polaritons (SPPs) in graphene [24–26], to surface phonon polaritons (SPhPs) in polar dielectric films [27, 28], may help bridge this length scale discrepancy [29] as a result of their extremely short wavelengths, predicted to potentially be as low as just a few nanometers. The confinement of the electromagnetic field in both conventional and more recent SP(h)P materials enables these modes to be the framework for applications such as more efficient energy transfer mechanisms [30, 31], graphene based protein sensors [32], radiation sources [16, 33–35], light-based devices [36] as well as sub-diffraction limit resolution microscopy [37, 38].

In this paper we show that by imbuing SP(h)P modes with OAM we raise the possibility of tailoring the selection rules for absorption in a way that highly forbidden transitions can be accessed and controlled. We find that these vortex modes enable new selection rules based in part on the conservation of angular momentum, providing a new scheme for the control of electronic transitions in a variety of electronic systems. We can use vortices to allow conventionally forbidden transitions to be fast and dominant and we can also use vortices to prevent conventionally allowed transitions from being dominant. We also show the robustness of this scheme by studying the effect of off-axis displacements relative to the center of a polaritonic vortex. For large displacements of the electronic system we study how the dominance of different absorption processes depends on its radial displacement. We find the surprising result that even when the atom is off-center relative to the vortex (i.e., when angular momentum conservation doesn’t hold), it is possible to make non-angular-momentum-conserving forbidden transitions dominant. Thus, by controlling the placement of the emitter, different transitions may be studied. With future experimental realizations in mind, we show how the increase of the confinement of the mode can lead to an enhancement of the absorption rates of the atom-like system at the expense of lower robustness. This is of particular interest in 2D conductors like graphene where the confinement factor of these polaritonic excitations can be externally tuned [25, 39].

To arrive at these results, we developed a unified quantum mechanical formalism for understanding the interaction between electrons and vortex polaritons, considering absorption and emission processes involving one vortex polariton and even pairs of entangled vortex polaritons. We consider spontaneous emission in addition to absorption because knowledge of such a process would be instrumental in efforts to study quantum optics with OAM-carrying polaritons. We explicitly develop the consequences of this formalism for the interaction of atoms with OAM polaritons such as 2D plasmons and hyperbolic polaritons in hexagonal boron nitride.

## II. CLASSICAL AND QUANTUM ELECTRODYNAMICS OF POLARITONIC VORTICES

OAM carrying SP(h)P modes are most naturally understood as a superposition of plane SP(h)P modes. These plane modes are adequately described in the framework of classical electrodynamics by evanescent waves propagating at the material surface. In a gauge where the scalar potential identically vanishes, the fields are fully described by the vector potential, which in the electrostatic limit is given by [40]:

$$\mathbf{A}_{\mathbf{q}} = \frac{A_0}{\sqrt{2}} (\hat{q} + i\hat{z}) e^{-qz} e^{i(\mathbf{q}\cdot\boldsymbol{\rho} - \omega t)}, \quad (1)$$

where  $\mathbf{q}$  corresponds to the in-plane wave vector of the mode (whose magnitude matches the out-of-plane inverse decay length in the electrostatic limit),  $\boldsymbol{\rho}$  corresponds to the in-plane position,  $\omega$  is the angular frequency of the mode,  $\hat{z}$  direction is the out of plane direction,  $A_0$  is the amplitude of the field and hats correspond to unit vectors. To fully describe SP(h)P modes, it is necessary to determine the dispersion relation  $\mathbf{q}(\omega)$ . Often a simple (local) Drude model suffices to obtain good agreement with the experimental results; however more involved methods, such as the random phase approximation, may be necessary for a better quantitative understanding of the system [40–43].

In order to compare and quantify the confinement of the electromagnetic radiation we define the confinement factor,  $\eta$ , as the ratio between the wavelength of free-space radiation and the wavelength of an SP(h)P mode of equal frequency. The confinement factor is extracted from the dispersion relation as  $q = \eta\omega/c$  with  $\eta = \eta(\omega)$  and provides a figure of merit for comparing different SP(h)P supporting materials. For light-matter interactions, we show that just knowing the confinement factor already gives a good order-of-magnitude estimate of the strengths of various light-matter interactions, in consistency with [29]. The range of relevant materials and associated confinement factors is vast and includes SPhP modes in SiC, where  $\eta$  can experimentally reach values of 200 [44]; SPhP modes in hBN, where  $\eta$  has been experimentally observed to be near 100 [45] and where theoretical upper bounds greater than 1000 are predicted by a spatially local model of the SPhP dispersion [46]; SPP modes in monolayer metal films like silver and beryllium, where  $\eta$  can reach values around 300 [47] and 350 [48] respectively (although with very large losses); and SPP modes in graphene, where measurements of  $\eta$  fall in the range of 150-240 [40, 49–51] for different regimes and where theoretical upper bounds are around 300 [40]. Using experimentally

observed confinement factors, recent theoretical studies have predicted a dramatic increase in the decay rate of excited states of nearby SP(h)P supporting materials [29, 52].

Having reviewed the basic properties of plane-wave polaritons, an OAM carrying (vortex) mode can then be easily understood as a superposition of plane-wave modes whose phase shift is dependent on the incoming angle [53, 54]. The resulting radiation profile in the region above the polaritonic material can be written analytically as:

$$\begin{aligned} \mathbf{A}_{q,m} &= \frac{1}{2\pi} \int_0^{2\pi} d\alpha A_{\mathbf{q}} e^{im\alpha} \\ &= \frac{A_0}{2\sqrt{2}} e^{im\phi} e^{-q|z|} i^{m+1} \left( \hat{\rho}(J_{m+1}(q\rho) - J_{m-1}(q\rho)) - i\hat{\phi} \frac{2mJ_m(q\rho)}{q\rho} + \hat{z} 2J_m(q\rho) \right), \end{aligned} \quad (2)$$

where  $\rho$ ,  $\phi$  and  $z$  are cylindrical coordinates defined around the vortex center,  $J_m(\rho)$  is the Bessel function of the first kind (of order  $m$ ) and  $\alpha$  is the angle between  $\mathbf{q}$  and some reference direction, set to be  $\hat{x}$  without loss of generality. The full derivation can be found in the Supplementary Material (SM), in agreement with the prediction in [55] for graphene SPPs.

The resulting phase winding gives rise to an OAM of  $\hbar m$ , where  $m$  is an integer. In the SM, we show a unified approach to compute (and normalize) vortex modes in any polaritonic material sustaining highly confined modes. In addition to deriving results for graphene, we derive explicit results for the case of hBN, whose hyperbolic polaritons have been of much recent interest. It is worth noting that these shaped polaritonic fields have been realized in silver and gold through the use of slit based coupling [53, 54, 56]. Thus the same procedure should be applicable to other classes of plasmonic materials, where the confinement factors can be much larger. As we shall soon show, it is precisely this large confinement that will allow for the possibility of controlling atomic transitions using angular momentum.

Having written the vortex modes, we can now quantize them and write down electromagnetic field operators and their Hamiltonian in the basis of vortex modes.

$$\begin{aligned} H &= H_{\text{ele}} + H_{\text{SP(h)P}} + H_{\text{int}} \quad \text{with} \\ H_{\text{int}} &= \frac{e}{2m_e} (\mathbf{A} \cdot \mathbf{p} + \mathbf{p} \cdot \mathbf{A}) + \frac{e^2}{m_e^2} \mathbf{A}^2 \quad \text{where} \\ \mathbf{A} &= \sum_{q,m} \sqrt{\frac{\hbar q^2}{4\bar{\epsilon}_r \epsilon_0 \omega_q L \xi_q}} (\mathbf{F}_{q,m} \hat{a}_{q,m} + \mathbf{F}_{q,m}^* \hat{a}_{q,m}^\dagger) \end{aligned} \quad (3)$$

and  $H_{\text{ele}}$  corresponds to the Hamiltonian of the electron,  $H_{\text{SP(h)P}}$  corresponds to the Hamiltonian corresponds to the free SP(h)P modes, and  $H_{\text{int}}$  to the interaction between the two.  $m_e$  and  $e$  are

the mass and charge of the electron,  $\epsilon_0$  the vacuum permittivity,  $\bar{\epsilon}_r$  the average relative electric permittivity of the dielectric above and below the interface and  $L$  the normalization length of the system.  $\hat{a}_{q,m}$  ( $\hat{a}_{q,m}^\dagger$ ) are the annihilation (creation) operators of the field mode with vector profile  $\mathbf{F}_{q,m}$ , as described in the SM. The parameter  $\xi_q$  is a dimensionless normalization factor which is required for the energy of the vortex mode to be  $\hbar\omega$ . We adopt a convention in the SM such that  $\xi_q = 1$  for graphene plasmons at all values of  $q$ . We emphasize here that  $\xi$  and  $v_g$  (the group velocity) are the only factors that differ between different polaritonic materials with the same geometry. That is because the functional form of the vortex modes in the region above the polaritonic material is always the same for a slab geometry. The factor  $\xi v_g$  in other polaritonic materials with the same value of confinement will generally be similar to that of graphene, meaning that we can understand the strength of light-matter interactions with vortices almost entirely in terms of the confinement factor. In the SM, we explicitly discuss the role of the  $\xi$  and  $v_g$  factors for 2D plasmonic materials and for hBN. In Figure (S1) of the SM, we compare the  $\xi v_g$  of hBN (for the fundamental branch in the upper Reststrahlen band) to that of graphene as a function of polaritonic confinement and find that they are consistently of the same order of magnitude. This automatically means that our claims about the ability to control forbidden transitions using polaritonic vortices hold just as well for hBN as they do for graphene. This may be of interest given the relatively low losses of phonon polaritons in hBN.

The reason behind the quantum treatment of the problem (as opposed to a semi-classical treatment) arises from the extendability of this approach. This formalism enables us, for example, to consider absorption and spontaneous emission (at any order in quantum electrodynamics) in the same framework, which is clearly not possible classically. Moreover it connects absorption at the single-polariton level to the Purcell factor, thus allowing one to easily understand absorption through the Purcell factor. In the SM, we derive general expressions for absorption and spontaneous emission of polaritonic vortex modes by electronic systems up to second-order in perturbation theory, providing tools by which to pursue further interesting directions in the quantum optics of shaped polaritons. As an explicit example, in the SM we analyze two-polariton emission processes in the OAM basis. In the main text of the paper, we focus purely on the absorption of vortex polaritons at first-order perturbation theory and derive the corresponding transition rates using Fermi's Golden Rule. The higher order term  $\mathbf{A}^2$  is neglected in this analysis, since, to lowest order, it only provides an overall constant correction to the energy of the system and it is not responsible



for the transition between different electronic states. Finally, we point out that the choice of a hydrogen atom as the absorber is for theoretical simplicity and to further illustrate our results with a specific example. Our calculations can readily be extended to other atomic, molecular, and solid-state systems. In an experiment, one may likely opt for an electronic system whose position over the vortex can be controlled very precisely, such as quantum dots or quantum wells. To this end, we start our analysis by ignoring the motion of the electronic system (as is quite commonly done). Then we provide a means for analyzing interactions between atoms and vortices when there is considerable uncertainty in the position of the atom.

### III. TUNABLE SELECTION RULES

In this work we consider the absorption transitions of an electron in a hydrogen atom located a height  $z_0$  above a surface supporting OAM carrying SP(h)P modes, as depicted in Figure (1). Computing the absorption rates, we describe new selection rules that arise in this system and their robustness to the displacement of the atom's position relative to the vortex center. Throughout this paper we take as an example the family of transitions from initial principal quantum number 5 to final principal quantum number 6. Because of the wide range of possible transitions, both dipole allowed and forbidden, we can illustrate both enhancement and control over transitions via a wide variety of examples. Nevertheless, the properties reported in this study are not unique to this family of transitions or to this specific electronic system, and similar qualitative results arise in other transition families and in other atom-like systems.

Computing the absorption rate for the case where the atom is aligned with the vortex center, for different electronic transitions and vortex modes, we obtain the results shown in Figure (2). Throughout this paper, our calculations refer to the absorption rates of a single photon. Within the Fermi Golden rule, the transition rate is proportional to the number of photons in the system which enables direct generalization of our results. These results make evident the selection rules associated with the conservation of angular momentum:

$$\Delta m = m_{\text{vortex}} \quad (4)$$

where  $\hbar\Delta m$  is the change in z-projected angular momentum of the electron and  $\hbar m_{\text{vortex}}$  is the OAM of the vortex mode. By generating a SP(h)P vortex mode, we are able to control the electronic transitions of the atom, for arbitrarily large values of  $\Delta m$ . This selection rule is exact and

arises from the requirement that the azimuthal phase term of the mode ( $e^{im_{\text{vortex}}\theta}$ ) and the orbital wavefunction product ( $e^{-i\Delta m\theta}$ ) must cancel for the interaction matrix element to be non-zero. This (mis)match of phase between the vortex mode and atomic degrees of freedom is illustrated in the phase plots on the right side of Figure (2), corresponding to different highlighted transitions on the left plot.

The impact of the confinement factor on the transitions rates is also of importance as it guides the choice of material for possible future experiments. A greater confinement leads to an increase in the absorption rate by many orders of magnitude in dipole forbidden transitions, as higher multipole terms of the interaction become allowed [29]. For example, for the dipole forbidden transition  $(5, 0, 0) \rightarrow (6, 4, 0)$  transition, an E4/hexadecapole transition, the increase of the confinement factor from 2 to 250 leads to an increase in the transition rate from an event every many 100's of years to one every 10  $\mu\text{s}$ . By coupling to higher multipole modes of radiation the allowed transitions are only constrained by the conservation of angular momentum described in Equation (4). All the transitions fulfilling this condition yield non-zero transition rates, albeit with different magnitudes.

However, in real experimental systems we expect the rotational symmetry, responsible for the selection rules of Equation (4), to be broken by the uncertainty in the placement of the atom. It is then important to understand the robustness of the new selection rules as the symmetry of the system is broken by the displacement of the atom with respect to the vortex center. When analyzing the absorption rate as a function of the position of the atom we find, as one would expect, that the selection rule no longer applies exactly, but that the corresponding transition is still the dominant process near the center, as shown in Figs.(3,4). However, surprisingly, this dominance occurs over a displacement of the order of the wavelength of the mode rather than, as one might expect, the size of the electronic system.

This result can be understood by considering the vortex (displaced relative to the atom) as a superposition of vortex modes centered at the atom. The linearity of the interaction matrix element with respect to the field implies that only a single vortex mode (satisfying Equation (4)) will contribute to the absorption rate. Since the expansion of the vortex mode is independent of the electronic system in consideration the wavelength of the mode is the only length scale that can determine the dependence of the absorption rate with distance.

In particular the overlap between a vortex mode with OAM of  $\hbar m_{\text{vortex}}$  displaced by  $\mathbf{D}$  and

an atom-centered vortex mode of OAM  $\hbar n$  has magnitude  $|J_{n-m_{\text{vortex}}}(qD)|$ , where  $q$  is the in-plane momentum of the mode. This arises from the properties of the Bessel functions and its full derivation can be found in the SM. The absorption rates in the displaced case can then be simply calculated as:

$$\Gamma_{\Delta m, m_{\text{vortex}}}^D = J_{\Delta m - m_{\text{vortex}}}^2(qD) \Gamma_{\Delta m, \Delta m}^0 \quad (5)$$

where  $\Gamma_{\Delta m, m_{\text{vortex}}}^D$  is the transition rate between levels with  $\hbar \Delta m$  change in the z-projected angular momentum of an electronic system at  $D$  due to a vortex with charge  $m_{\text{vortex}}$ .  $\Gamma_{\Delta m, \Delta m}^0$  corresponds to the angular momentum conserving transition rate in a vortex centered electronic system and is defined as the baseline transition rate.

This analysis yields an even more surprising qualitative result; for special values of  $D$  where  $J_{\Delta m - m_{\text{vortex}}}(qD) = 0$ , a transition characterized by  $\Delta m$  is truly forbidden. In other words for every transition (even  $m_{\text{vortex}} = \Delta m$ ) there are concentric rings with radii of the order of the wavelength where the transition is truly forbidden.

The transitions from a system initially in the state (5,0,0) as a function of the displacement  $D$  of the atom from the vortex center are studied in the left column of Figure (3), where each row corresponds to a different value of OAM  $\hbar m_{\text{vortex}}$  carried by the vortex mode. Although for  $D = 0$  the selection rule Equation (4) is always satisfied and nearby the center of the vortex this transition is always dominant, increasing  $D$  yields a much richer landscape of transition rates, which is qualitatively different for different  $m_{\text{vortex}}$ . This fact implies that, given a single vortex mode, it is possible to tune the dominant transition using the radial position of the electronic system, providing an extra degree of freedom to control light-matter interactions. The fact that the absorption rate can be separated into a baseline rate, which specifies the scale of the transition rate, and an oscillatory Bessel term, which determines the displacement dependence, enables a simple yet powerful understanding of the relationship between different absorption rates. In particular, since the coefficients  $J_{\Delta m - m_{\text{vortex}}}(qD)$  have different zeros for any two different values of  $\Delta m$ , there are always regions where one transition dominates over the other.

#### IV. DISCUSSION

The previous discussion provides a framework for understanding a single atom-like system, whose position is known perfectly. However, in a real experimental setting there is always some

inherent uncertainty associated with the position of the atom. Other experimental challenges arise from the manipulation and preparation of the system, as well as the measurement of a meaningful spectroscopic signal from a single atom. To overcome these challenges, experimental realizations may require introducing more than one atom per vortex mode, or fabricating a sample that supports an array of vortices, as schematically pictured in the inset of Figure (4). In particular, the recent realization of geometries where the SPP energy is fully localized inside the coupling grating [56] provides the platform to make this technique a viable option for increasing the measured signal without interaction between nearby vortex modes.

The before-mentioned position uncertainty can be modeled through a probability distribution over the position of the atom. In this work we consider the radially uniform distribution of radius  $R$  around the vortex center, which, despite its simplicity, provides the same qualitative results as other, more complex, vortex centered distributions. In the right column of Figure (3), the expected absorption rate is computed for such distributions as a function of  $R$ . The impact of the probability distribution can be understood as smoothing the single atom absorption rates, leading to two major consequences: regions of dominance of transitions where  $\Delta m \neq m_{\text{vortex}}$  are moved further away from the center, making transitions with  $\Delta m = m_{\text{vortex}}$  more robust; and as  $R$  increases, processes with larger baseline transition rates become dominant as the oscillatory behavior from the Bessel function coefficient is averaged out.

As mentioned before, the results presented here are not unique to the transitions in use, but are general considerations for all sets of transitions. In order to demonstrate the robustness of the selection rules for even larger  $\Delta m$ , which are normally highly suppressed in the dipole regime, we investigate in Figure (4) the absorption of a vortex mode with  $m_{\text{vortex}} = 5$ . As in Figure (3), the left column corresponds to the calculation of the absorption rate for single atomic system, while the right column corresponds to the absorption rate over a uniform distribution of radius  $R$  of the position of the atom. As expected, the dominance of the  $\Delta m = 5$  transition is present for small radii, despite having a baseline rate many orders of magnitude smaller than the remaining transitions. As the atom moves away from the center of the vortex, the dominant transition generally has a smaller  $\Delta m$ , because a vortex of smaller angular momentum gives rise to a larger baseline transition. The same smoothing observed in Figure (3) is present in this case, which enables us to predict the measured absorption rate for a given experimental atom placement uncertainty. These two plots only contain the transitions which are dominant at some radius; for

a complete plot with all the transitions from  $(5, 0, 0) \rightarrow (6, l, m)$ , refer to Figure (7) of the SM.

To fully characterize the transition dynamics it becomes important to also consider the impact of the confinement factor on the absorption rates and their robustness. As shown in Figure (2) the increase in the confinement of the material leads to an increase of the absorption rates of the atom. However, it is also associated with an exponential decrease of the value of the field at the location of the atom, due to the evanescent nature of the mode. The competition between these two effects leads to a peak in the absorption rate after which the exponential suppression of the modes counteracts the increase in confinement, as illustrated in Figure (5). Another consequence of the increase in confinement factor is the decrease in the length scale of the SP(h)P modes, which leads to a decrease in the size of the regions where the transitions of interest are meaningfully dominant, requiring a greater experimental precision. This creates a trade-off between higher absorption rate and lower displacement tolerance. Understanding the impact of the confinement factor in the experiment is of special interest in graphene, where the confinement factor of SPP can be externally tuned [25], providing an extra degree of freedom for optimizing the experimental setup.

Although the discussion in this paper covers SP(h)P mode, these results can be straightforwardly extended to plasmons in conventional metals interfaced with larger atoms, or other atom-like systems like quantum dots. In this case, the length scales between the wavelength of light and the electronic system are matched not only by confining light, but also by considering larger electronic systems (e.g. quantum dots) [57]. Within these quantum dots, whose size is comparable to that of the SPP mode, the discussion and results presented in this paper also apply. By constructing analogous OAM carrying SP(h)P modes we obtain the same selection rules and properties described in this paper.

Although in this work we only considered electronic systems with spherical symmetry, Equation (4) arises from the continuous rotation symmetry around the SP(h)P evanescent directions ( $\hat{z}$ ) which ensure that the z-projected angular momentum is a good quantum number. Even more generically than that, vortices will lead to non-trivial selection rules even for systems with merely parity or discrete rotational symmetries.

One consideration missing from our discussion is the presence of losses in the materials. However it was shown [29] that for a wide range of parameters, including those of interest in this work (large confinement factors), the transition rates are insensitive to losses, even for quality factors as low

as 5. Our formalism can be generalized to include material losses as shown in a previous work [29], allowing our results to be extended to an even wider range of materials.

## V. CONCLUSION

In this paper we have shown how orbital angular momentum carrying polaritonic vortex modes can be used to selectively induce electronic transitions in nearby electronic systems. We showed how new selection rules, corresponding to angular momentum conservation, arise when the atom-like system is aligned with the center of the vortex mode. In the off-centered case, we showed how the transition that conserves angular momentum ( $\hbar\Delta m = \hbar m_{\text{vortex}}$ ) is always dominant near the center. For larger displacements of the electronic system, different transitions become dominant within displacements of the order of the wavelength of the mode as opposed to, as one would expect, the electronic orbital length scale. As a result, by varying the radial position of our electronic system, a single SP(h)P vortex mode is able to access a variety of novel transitions.

The results presented in this work have important implications both experimentally and theoretically. The ability to generate masks in substrates which support an OAM carrying vortex SPP has already been demonstrated [53, 54, 56]. Fabricating an array of such masks provides the first step towards an experimental setup capable of observing and further expanding the ideas presented in this paper. These suggest several exciting directions for future research. Of great interest is the study and engineering of other slit geometries (beyond vortex producing geometries), which may lead to shaped field profiles with more complex and exotic selection rules, providing a general platform for the control and generation of quantum states in atom-like systems.

An interesting direction of research will be finding alternative sources of shaped polaritons (such as vortex modes), that can be applied to cases where creating a mask may prove to be challenging. One interesting possibility is using electronic systems whose bound states have cylindrical (not spherical) symmetry, such as an idealized quantum dot. Due to the angular momentum quantum number of the initial and final electronic states, these cylindrical emitters can potentially emit modes of a fixed orbital angular momentum, acting as sources of angular momentum modes on the single-photon scale. One can use the same cylindrical emitter to generate different OAM photons by tailoring the Purcell factor to have large peaks associated with different transitions of the same emitter (which each can be associated with different changes in orbital angular momentum). These

single-polariton sources can then be potentially interfaced with absorbers.

In the long term, the ability to engineer the electronic transitions in a quantum system, enabled by polaritonic modes, opens the doors for many applications which depend on usually inaccessible quantum states. Generating these quantum states in simple table-top settings leads to novel light emitting devices and even lasing technologies, by enabling new decay paths in quantum systems. At the same time, including OAM carrying polariton modes in the toolbox of spectroscopists adds a new technique with which to probe and investigate electronic transitions and states, in particular in multi-electron systems, where the large degeneracy of the states is lifted and an even greater control over the electronic transitions is allowed.

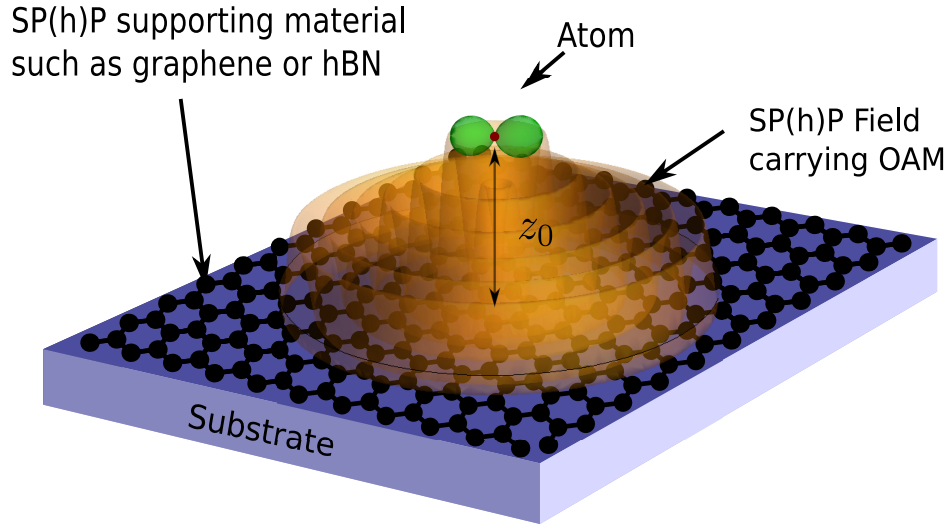


**FIG. 1: Illustration of an Atomic System Coupled to Polaritonic Vortices.** An electronic system, such as an atom, is placed a height  $z_0$  above the center of an OAM carrying polaritonic vortex mode, exciting transitions via new selection rules.



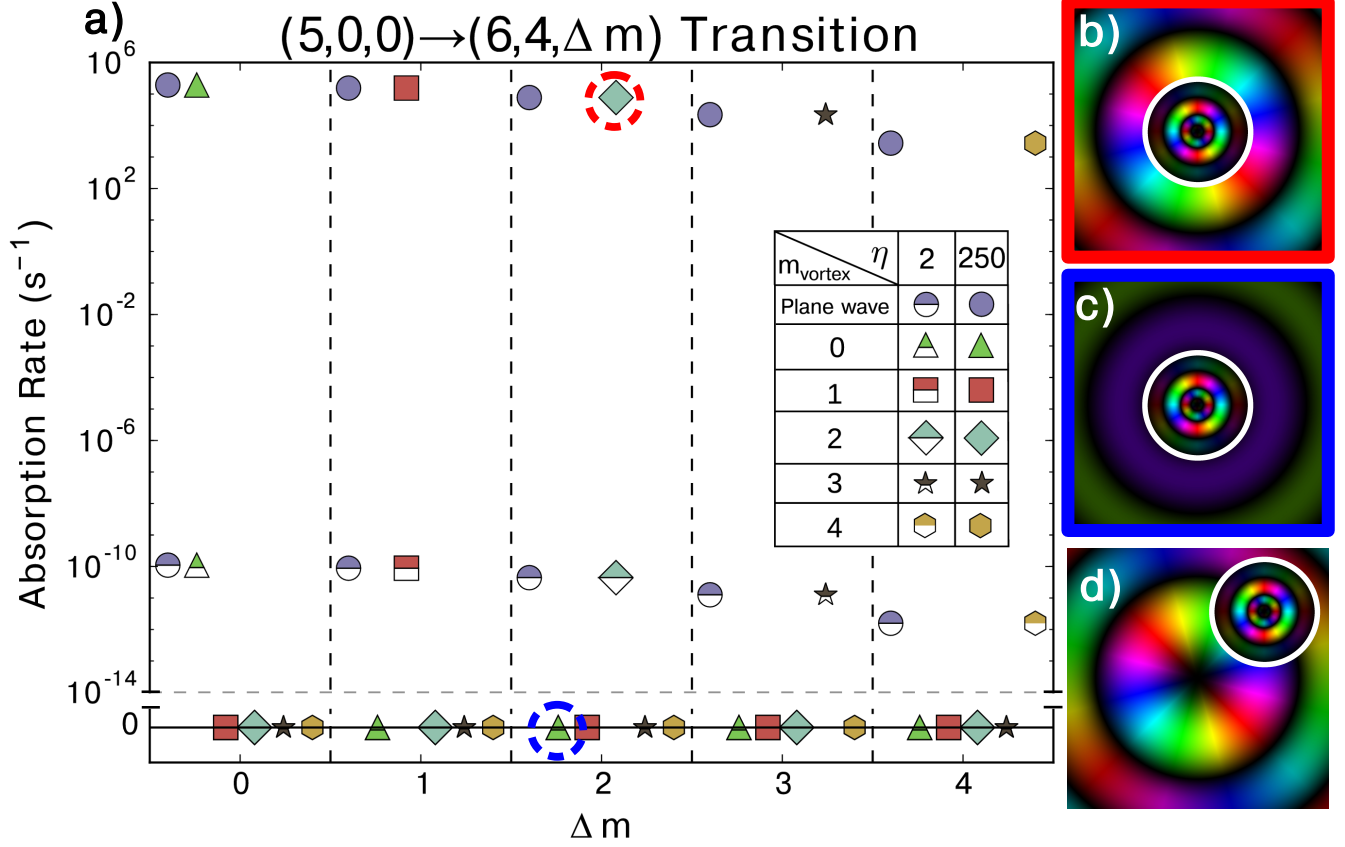


FIG. 2: **Selection Rules in the absorption of OAM carrying SP(h)P modes.** **a)** Calculation of the absorption rate due to a planar SP(h)P and an OAM carrying vortex SP(h)P for different transition in the family  $(5,0,0) \Rightarrow (6,4,\Delta m)$  for two different values of confinement factor  $\eta$ , 2 (half-filled) and 250 (filled), with  $z_0 = 20$  nm. The vortex modes impose selection rules on the electronic transitions, while the increase in confinement factor leads to an improvement of the absorption rate by a factor of  $\sim 10^{15}$ . The examples of  $\eta = 2$  show that, although free space OAM carrying modes could in principle impose the same selection rules, the difference in length-scales between radiation and the atom size results in absorption rates too small for experimental observation. The absorption rates are normalized by assuming the SP(h)P modes carries a single photon quanta. **b)** and **c)** the phase plots of the highlighted transitions of equal color, where the inside (outside) of the circle corresponds to the electron orbital components (vortex mode). The size of the atom was artificially increased tenfold for illustration purposes. **d)** the phase plot where the rotation symmetry has been broken by the atom's displacement from the center of the vortex mode.

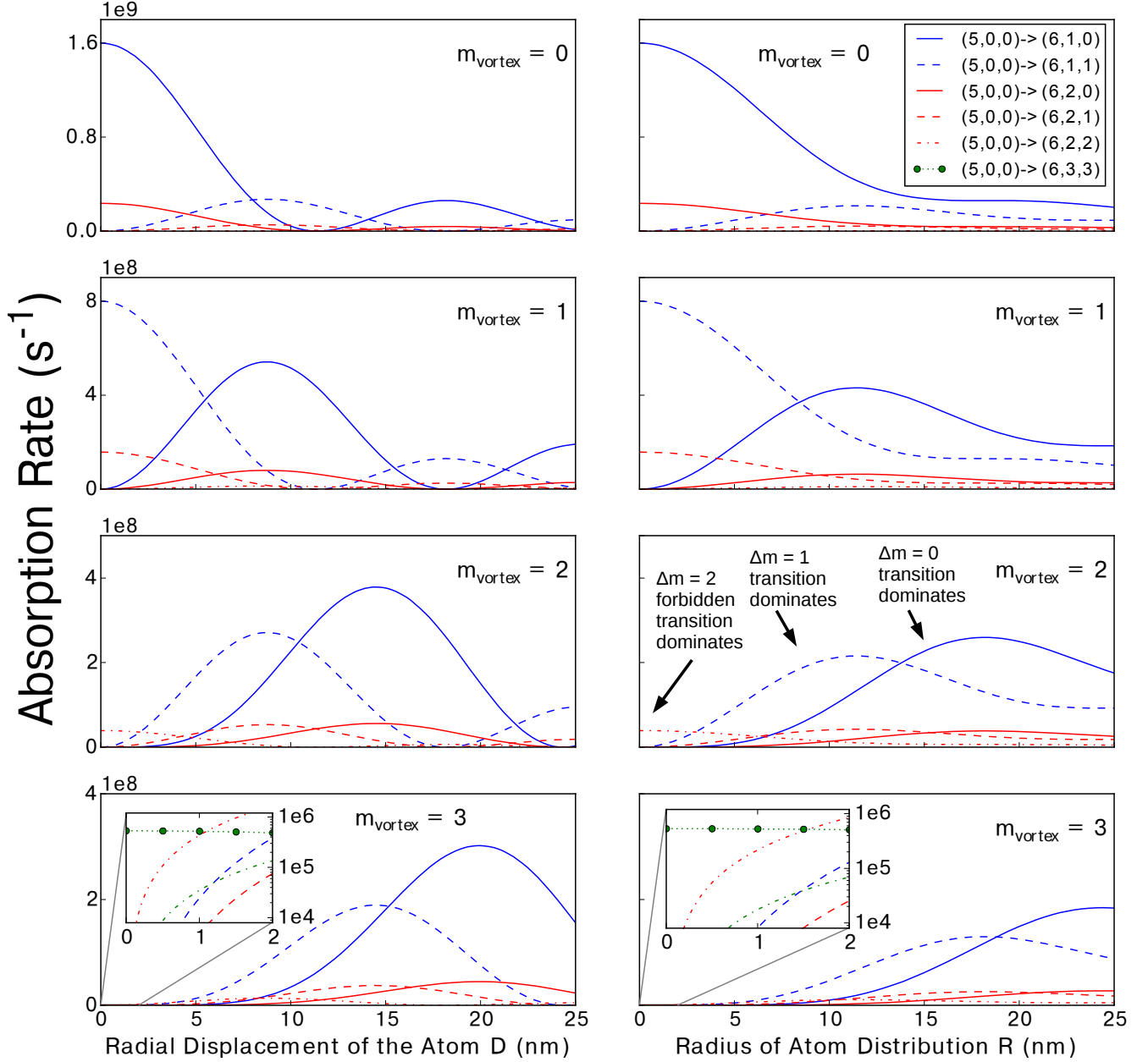


FIG. 3: **Robustness of the angular momentum selection rules to atom displacement.** Dependence of the absorption rates of a displaced individual atom (left column) and uniform atomic distribution (right column) for transitions with initial state  $(5,0,0)$  and final principal quantum number 6 at a confinement factor of  $\eta = 250$  and  $z_0 = 20$  nm. As the rotational symmetry is broken, the selection rule discussed in Figure (2) is no longer valid and all  $\Delta m$  transitions become allowed. The absorption rates match the selection rule of Equation (4) at  $D = 0$ , and for small  $D$  this transition always dominates. For larger  $D$ , other transitions can become dominant, as the value of  $J_0(qD)$  decreases and higher order Bessel terms become comparable.

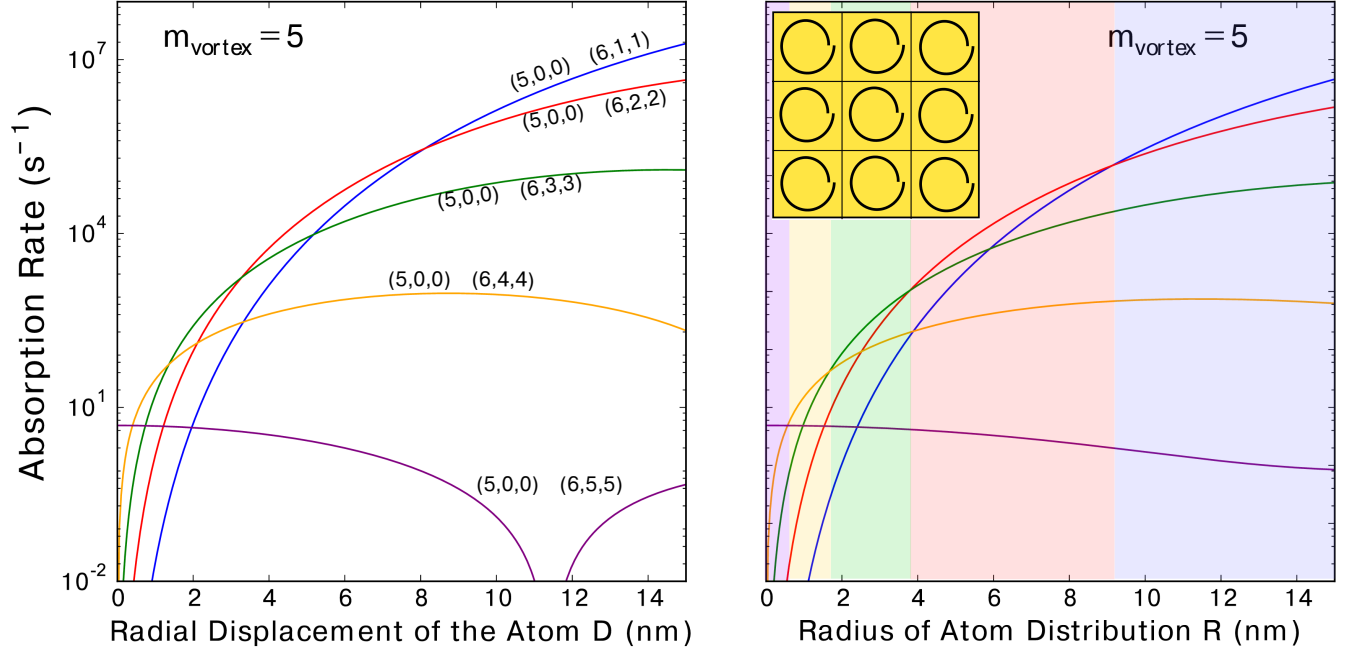


FIG. 4: **Absorption rates for a highly suppressed transition.** Using the same parameters as in Figure (3), the absorption of  $m_{\text{vortex}} = 5$  SP(h)P modes is computed. The left column presents the absorption rates as a function of the atom displacement  $D$  while the right column presents the rates as a function of the radius  $R$  of an uniform distribution of the position of the atom. The colored regions represent the dominance of the differently colored transitions. The measured signal can be improved by performing many parallel experiments on a single substrate, as pictured in the inset schematic, based on the slit based vortex mode supporting geometries explored in [53, 54, 56]

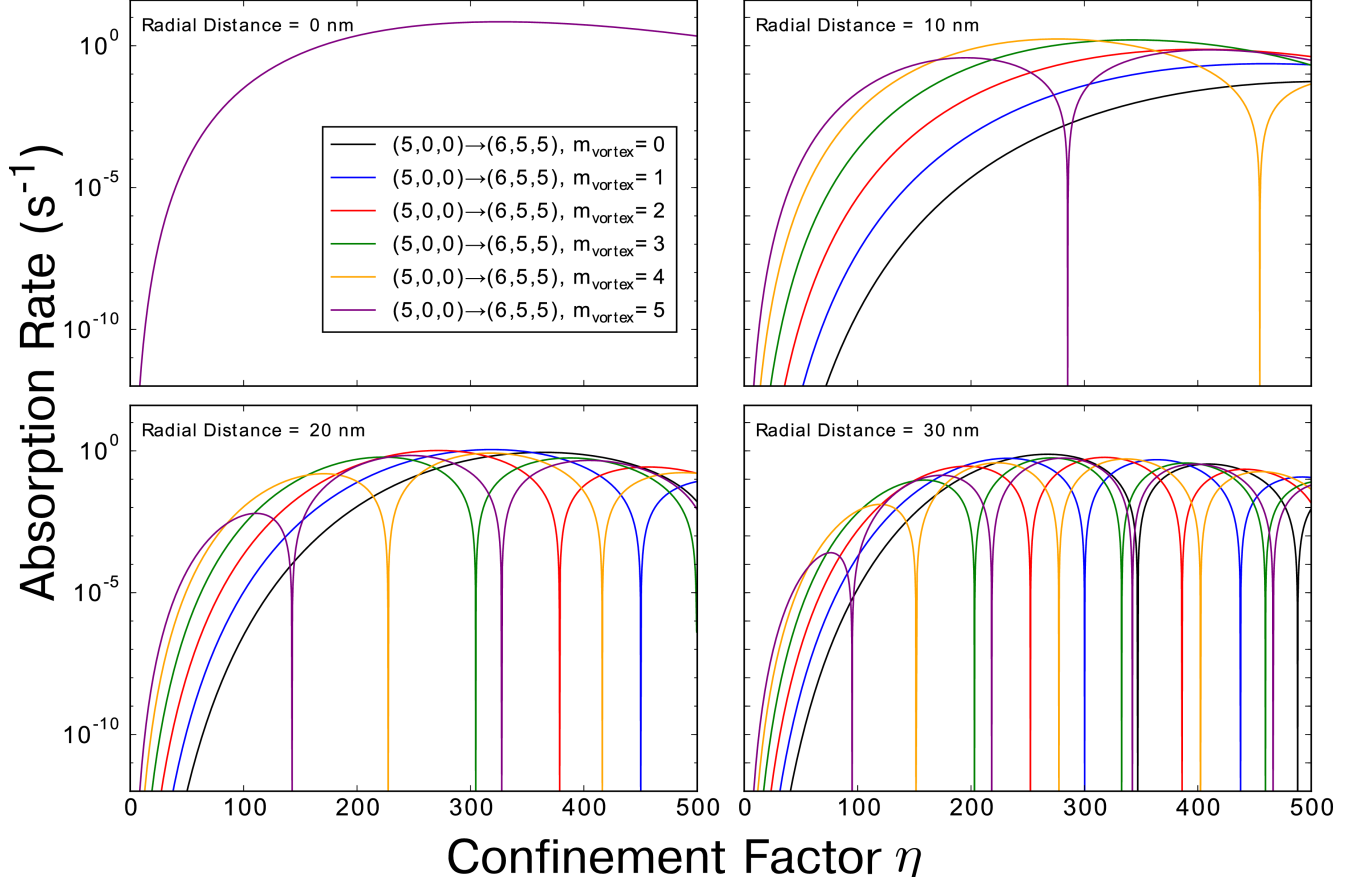


FIG. 5: **Impact of confinement factor on the absorption rate of a SP(h)P mode.** For different values of displacement distance (0,10,20,30 nm) the absorption rate between (5, 0, 0) and (6, 5, 5) electronic states for an hydrogen atom at  $z_0 = 20$  nm is plotted as a function of the confinement factor of the SP(h)P mode and for different vortex modes. The higher confinement factor leads to an increase in the absorption rate until the exponential decay of the field strength becomes dominant and diminishes the enhancement. At the same time, the increase in confinement factor leads to a decrease of the systems length scale, as observed by the greater density of absorption rate zeros (dips) at higher confinement factors. As a result, higher confinement factor requires a greater experimental precision to ensure the atom is in the region where the transition of interest is dominant. The zeroes of the rates will be regulated by losses, which lead to an averaging over wavevectors.

- 
- [1] L. Allen, M. W. Beijersbergen, R. J. C. Spreeuw, and J. P. Woerdman, “Orbital angular momentum of light and the transformation of Laguerre-Gaussian laser modes,” *Physical Review A*, vol. 45, pp. 8185–8189, jun 1992.
  - [2] H. He, M. Friese, N. Heckenberg, and H. Rubinsztein-Dunlop, “Direct observation of transfer of angular momentum to absorptive particles from a laser beam with a phase singularity,” *Physical review letters*, vol. 75, pp. 826–829, jul 1995.
  - [3] M. P. J. Lavery, F. C. Speirits, S. M. Barnett, and M. J. Padgett, “Detection of a spinning object using light’s orbital angular momentum,” *Science (New York, N.Y.)*, vol. 341, pp. 537–40, aug 2013.
  - [4] Y. Yan, G. Xie, M. P. J. Lavery, H. Huang, N. Ahmed, C. Bao, Y. Ren, Y. Cao, L. Li, Z. Zhao, A. F. Molisch, M. Tur, M. J. Padgett, and A. E. Willner, “High-capacity millimetre-wave communications with orbital angular momentum multiplexing,” *Nature communications*, vol. 5, p. 4876, jan 2014.
  - [5] J. Wang, J.-Y. Yang, I. M. Fazal, N. Ahmed, Y. Yan, H. Huang, Y. Ren, Y. Yue, S. Dolinar, M. Tur, and A. E. Willner, “Terabit free-space data transmission employing orbital angular momentum multiplexing,” *Nature Photonics*, vol. 6, pp. 488–496, jun 2012.
  - [6] H. Ren, X. Li, Q. Zhang, and M. Gu, “On-chip noninterference angular momentum multiplexing of broadband light,” *Science (New York, N.Y.)*, vol. 352, pp. 805–809, apr 2016.
  - [7] G. Molina-Terriza, J. P. Torres, and L. Torner, “Twisted photons,” *Nature Physics*, vol. 3, pp. 305–310, may 2007.
  - [8] A. Nicolas, L. Veissier, L. Giner, E. Giacobino, D. Maxein, and J. Laurat, “A quantum memory for orbital angular momentum photonic qubits,” *Nature Photonics*, vol. 8, pp. 234–238, jan 2014.
  - [9] A. Mair, A. Vaziri, G. Weihs, and A. Zeilinger, “Entanglement of the orbital angular momentum states of photons,” *Nature*, vol. 412, pp. 313–6, jul 2001.
  - [10] M. Mirhosseini, O. S. Magaña-Loaiza, M. N. O’Sullivan, B. Rodenburg, M. Malik, M. P. J. Lavery, M. J. Padgett, D. J. Gauthier, and R. W. Boyd, “High-dimensional quantum cryptography with twisted light,” *New Journal of Physics*, vol. 17, p. 033033, mar 2015.
  - [11] M. Malik, M. Erhard, M. Huber, M. Krenn, R. Fickler, and A. Zeilinger, “Multi-photon entanglement in high dimensions,” *Nature Photonics*, vol. 10, pp. 248–252, feb 2016.
  - [12] K. Y. Bliokh, Y. P. Bliokh, S. Savel’ev, and F. Nori, “Semiclassical dynamics of electron wave packet

- states with phase vortices,” *Physical review letters*, vol. 99, p. 190404, nov 2007.
- [13] M. Uchida and A. Tonomura, “Generation of electron beams carrying orbital angular momentum,” *Nature*, vol. 464, pp. 737–9, apr 2010.
  - [14] J. Verbeeck, H. Tian, and P. Schattschneider, “Production and application of electron vortex beams,” *Nature*, vol. 467, pp. 301–4, sep 2010.
  - [15] B. J. McMorran, A. Agrawal, I. M. Anderson, A. A. Herzing, H. J. Lezec, J. J. McClelland, J. Unguris, L. Allen, M. W. Beijersbergen, R. J. C. Spreeuw, J. P. Woerdman, S. Fürhapter, A. Jesacher, S. Bernet, M. Ritsch-Marte, S. W. Hell, G. Foo, D. M. Palacios, J. Swartzlander, D. G. Grier, A. Mair, A. Vaziri, G. Weihs, A. Zeilinger, M. F. Andersen, S. Franke-Arnold, L. Allen, M. Padgett, K. Bliokh, Y. Bliokh, S. Savel’ev, F. Nori, M. Uchida, A. Tonomura, J. Leach, E. Yao, M. J. Padgett, J. Verbeeck, H. Tian, P. Schattschneider, B. McMorran, J. D. Perreault, T. A. Savas, A. Cronin, A. Cronin, B. McMorran, B. J. McMorran, A. D. Cronin, V. Y. Bazhenov, M. V. Vasnetsov, M. S. Soskin, N. R. Heckenberg, R. McDuff, C. P. Smith, H. Rubinsztein-Dunlop, M. J. Wegener, A. V. Volyar, V. G. Shvedov, T. A. Fadeeva, A. Jesacher, S. Fürhapter, S. Bernet, M. Ritsch-Marte, R. Danev, H. Okawara, N. Usuda, K. Kametani, K. Nagayama, K. Schultheiß, F. Pérez-Willard, B. Barton, D. Gerthsen, and R. R. Schröder, “Electron vortex beams with high quanta of orbital angular momentum,” *Science (New York, N.Y.)*, vol. 331, pp. 192–5, jan 2011.
  - [16] I. Kaminer, M. Mutzafi, A. Levy, G. Harari, H. Herzig Sheinfux, S. Skirlo, J. Nemirovsky, J. D. Joannopoulos, M. Segev, and M. Soljačić, “Quantum Čerenkov Radiation: Spectral Cutoffs and the Role of Spin and Orbital Angular Momentum,” *Physical Review X*, vol. 6, p. 011006, jan 2016.
  - [17] A. M. Yao and M. J. Padgett, “Orbital angular momentum: origins, behavior and applications,” *Advances in Optics and Photonics*, vol. 3, p. 161, may 2011.
  - [18] M. Babiker, C. Bennett, D. Andrews, and L. D. Romero, “Orbital angular momentum exchange in the interaction of twisted light with molecules,” *Physical review letters*, vol. 89, no. 14, p. 143601, 2002.
  - [19] A. Picón, A. Benseny, J. Mompart, J. R. Vázquez de Aldana, L. Plaja, G. F. Calvo, and L. Roso, “Transferring orbital and spin angular momenta of light to atoms,” *New Journal of Physics*, vol. 12, p. 083053, aug 2010.
  - [20] A. Picón, J. Mompart, J. R. V. de Aldana, L. Plaja, G. F. Calvo, and L. Roso, “Photoionization with orbital angular momentum beams,” *Optics express*, vol. 18, pp. 3660–71, feb 2010.

- [21] A. Afanasev, C. E. Carlson, and A. Mukherjee, “Off-axis excitation of hydrogenlike atoms by twisted photons,” *Physical Review A*, vol. 88, p. 033841, sep 2013.
- [22] A. Afanasev, C. E. Carlson, and A. Mukherjee, “High-multipole excitations of hydrogen-like atoms by twisted photons near a phase singularity,” *Journal of Optics*, vol. 18, no. 7, p. 074013, 2016.
- [23] C. T. Schmiegelow, J. Schulz, H. Kaufmann, T. Ruster, U. G. Poschinger, and F. Schmidt-Kaler, “Excitation of an atomic transition with a vortex laser beam,” *arXiv preprint arXiv:1511.07206*, 2015.
- [24] L. Ju, B. Geng, J. Horng, C. Girit, M. Martin, Z. Hao, H. A. Bechtel, X. Liang, A. Zettl, Y. R. Shen, and F. Wang, “Graphene plasmonics for tunable terahertz metamaterials,” *Nature Nanotechnology*, vol. 6, pp. 630–634, sep 2011.
- [25] J. Chen, M. Badioli, P. Alonso-González, S. Thongrattanasiri, F. Huth, J. Osmond, M. Spasenović, A. Centeno, A. Pesquera, P. Godignon, A. Z. Elorza, N. Camara, F. J. García de Abajo, R. Hillenbrand, and F. H. L. Koppens, “Optical nano-imaging of gate-tunable graphene plasmons,” *Nature*, vol. 487, pp. 77–81, jul 2012.
- [26] A. N. Grigorenko, M. Polini, and K. S. Novoselov, “Graphene plasmonics,” *Nature Photonics*, vol. 6, pp. 749–758, nov 2012.
- [27] S. Dai, Z. Fei, Q. Ma, A. S. Rodin, M. Wagner, A. S. McLeod, M. K. Liu, W. Gannett, W. Regan, K. Watanabe, T. Taniguchi, M. Thiemens, G. Dominguez, A. H. Castro Neto, A. Zettl, F. Keilmann, P. Jarillo-Herrero, M. M. Fogler, and D. N. Basov, “Tunable phonon polaritons in atomically thin van der Waals crystals of boron nitride,” *Science (New York, N.Y.)*, vol. 343, pp. 1125–9, mar 2014.
- [28] P. Li, M. Lewin, A. V. Kretinin, J. D. Caldwell, K. S. Novoselov, T. Taniguchi, K. Watanabe, F. Gaussmann, and T. Taubner, “Hyperbolic phonon-polaritons in boron nitride for near-field optical imaging and focusing,” *Nature Communications*, vol. 6, p. 7507, jun 2015.
- [29] N. Rivera, I. Kaminer, B. Zhen, J. D. Joannopoulos, and M. Soljačić, “Shrinking light to allow forbidden transitions on the atomic scale,” *Science (New York, N.Y.)*, vol. 353, pp. 263–9, jul 2016.
- [30] S. Shen, A. Narayanaswamy, and G. Chen, “Surface phonon polaritons mediated energy transfer between nanoscale gaps,” *Nano letters*, vol. 9, pp. 2909–13, aug 2009.
- [31] O. Ilic, M. Jablan, J. D. Joannopoulos, I. Celanovic, H. Buljan, and M. Soljačić, “Near-field thermal radiation transfer controlled by plasmons in graphene,” *Physical Review B*, vol. 85, p. 155422, apr 2012.

- [32] D. Rodrigo, O. Limaj, D. Janner, D. Etezadi, F. J. García de Abajo, V. Pruneri, and H. Altug, “APPLIED PHYSICS. Mid-infrared plasmonic biosensing with graphene.,” *Science (New York, N.Y.)*, vol. 349, pp. 165–8, jul 2015.
- [33] V. Apalkov and M. I. Stockman, “Proposed graphene nanospaser,” *Light: Science & Applications*, vol. 3, p. e191, jul 2014.
- [34] Y. D. Kim, H. Kim, Y. Cho, J. H. Ryoo, C.-H. Park, P. Kim, Y. S. Kim, S. Lee, Y. Li, S.-N. Park, Y. S. Yoo, D. Yoon, V. E. Dorgan, E. Pop, T. F. Heinz, J. Hone, S.-H. Chun, H. Cheong, S. W. Lee, M.-H. Bae, and Y. D. Park, “Bright visible light emission from graphene.,” *Nature nanotechnology*, vol. 10, pp. 676–81, aug 2015.
- [35] L. J. Wong, I. Kaminer, O. Ilic, J. D. Joannopoulos, and M. Soljačić, “Towards graphene plasmon-based free-electron infrared to X-ray sources,” *Nature Photonics*, vol. 10, pp. 46–52, nov 2015.
- [36] E. Ozbay, “Plasmonics: merging photonics and electronics at nanoscale dimensions.,” *Science (New York, N.Y.)*, vol. 311, pp. 189–93, jan 2006.
- [37] N. Fang, H. Lee, C. Sun, and X. Zhang, “Sub-diffraction-limited optical imaging with a silver superlens.,” *Science (New York, N.Y.)*, vol. 308, pp. 534–7, apr 2005.
- [38] S. Kawata, Y. Inouye, and P. Verma, “Plasmonics for near-field nano-imaging and superlensing,” *Nature Photonics*, vol. 3, pp. 388–394, jul 2009.
- [39] Z. Fei, A. S. Rodin, G. O. Andreev, W. Bao, A. S. McLeod, M. Wagner, L. M. Zhang, Z. Zhao, M. Thiemens, G. Dominguez, M. M. Fogler, A. H. Castro Neto, C. N. Lau, F. Keilmann, and D. N. Basov, “Gate-tuning of graphene plasmons revealed by infrared nano-imaging.,” *Nature*, vol. 487, pp. 82–5, jul 2012.
- [40] M. Jablan, H. Buljan, and M. Soljačić, “Plasmonics in graphene at infrared frequencies,” *Physical Review B*, vol. 80, p. 245435, dec 2009.
- [41] M. Jablan, M. Soljacic, and H. Buljan, “Plasmons in Graphene: Fundamental Properties and Potential Applications,” *Proceedings of the IEEE*, vol. 101, pp. 1689–1704, jul 2013.
- [42] J. Hofmann, E. Barnes, and S. Das Sarma, “Why does graphene behave as a weakly interacting system?,” *Physical review letters*, vol. 113, p. 105502, sep 2014.
- [43] A. F. Page, F. Ballout, O. Hess, and J. M. Hamm, “Nonequilibrium plasmons with gain in graphene,” *Physical Review B*, vol. 91, p. 075404, feb 2015.
- [44] J. D. Caldwell, O. J. Glembocki, Y. Francescato, N. Sharac, V. Giannini, F. J. Bezares, J. P. Long,



- J. C. Owrutsky, I. Vurgaftman, J. G. Tischler, V. D. Wheeler, N. D. Bassim, L. M. Shirey, R. Kasica, and S. A. Maier, “Low-loss, extreme subdiffraction photon confinement via silicon carbide localized surface phonon polariton resonators.,” *Nano letters*, vol. 13, pp. 3690–7, aug 2013.
- [45] J. D. Caldwell, A. V. Kretinin, Y. Chen, V. Giannini, M. M. Fogler, Y. Francescato, C. T. Ellis, J. G. Tischler, C. R. Woods, A. J. Giles, M. Hong, K. Watanabe, T. Taniguchi, S. A. Maier, and K. S. Novoselov, “Sub-diffractive volume-confined polaritons in the natural hyperbolic material hexagonal boron nitride.,” *Nature communications*, vol. 5, p. 5221, jan 2014.
- [46] A. Tomadin, A. Principi, J. C. W. Song, L. S. Levitov, and M. Polini, “Accessing Phonon Polaritons in Hyperbolic Crystals by Angle-Resolved Photoemission Spectroscopy.,” *Physical review letters*, vol. 115, p. 087401, aug 2015.
- [47] T. Nagao, T. Hildebrandt, M. Henzler, and S. Hasegawa, “Dispersion and damping of a two-dimensional plasmon in a metallic surface-state band.,” *Physical review letters*, vol. 86, pp. 5747–50, jun 2001.
- [48] B. Diaconescu, K. Pohl, L. Vattuone, L. Savio, P. Hofmann, V. M. Silkin, J. M. Pitarke, E. V. Chulkov, P. M. Echenique, D. Farías, and M. Rocca, “Low-energy acoustic plasmons at metal surfaces.,” *Nature*, vol. 448, pp. 57–9, jul 2007.
- [49] Y. Liu, R. F. Willis, K. V. Emtsev, and T. Seyller, “Plasmon dispersion and damping in electrically isolated two-dimensional charge sheets,” *Physical Review B*, vol. 78, p. 201403, nov 2008.
- [50] Z. Fei, G. O. Andreev, W. Bao, L. M. Zhang, A. S. McLeod, C. Wang, M. K. Stewart, Z. Zhao, G. Dominguez, M. Thieme, M. M. Fogler, M. J. Tauber, A. H. Castro-Neto, C. N. Lau, F. Keilmann, and D. N. Basov, “Infrared nanoscopy of dirac plasmons at the graphene-SiO<sub>2</sub> interface.,” *Nano letters*, vol. 11, pp. 4701–5, nov 2011.
- [51] A. Woessner, M. B. Lundberg, Y. Gao, A. Principi, P. Alonso-González, M. Carrega, K. Watanabe, T. Taniguchi, G. Vignale, M. Polini, J. Hone, R. Hillenbrand, and F. H. L. Koppens, “Highly confined low-loss plasmons in graphene-boron nitride heterostructures.,” *Nature materials*, vol. 14, pp. 421–5, apr 2015.
- [52] F. H. L. Koppens, D. E. Chang, and F. J. G. de Abajo, “Graphene Plasmonics: A Platform for Strong LightMatter Interactions,” 2011.
- [53] A. David, B. Gjonaj, Y. Blau, S. Dolev, and G. Bartal, “Nanoscale shaping and focusing of visible light in planar metaloxidesilicon waveguides,” *Optica*, vol. 2, p. 1045, dec 2015.

- [54] A. David, B. Gjonaj, and G. Bartal, “Two-dimensional optical nanovortices at visible light,” *Physical Review B*, vol. 93, p. 121302, mar 2016.
- [55] L. Du and D. Tang, “Manipulating propagating graphene plasmons at near field by shaped graphene nano-vacancies.,” *Journal of the Optical Society of America. A, Optics, image science, and vision*, vol. 31, pp. 691–5, may 2014.
- [56] G. Spektor, A. David, B. Gjonaj, G. Bartal, and M. Orenstein, “Metafocusing by a Metaspiral Plasmonic Lens.,” *Nano letters*, vol. 15, pp. 5739–43, sep 2015.
- [57] M. L. Andersen, S. Stobbe, A. S. Sørensen, and P. Lodahl, “Strongly modified plasmonmatter interaction with mesoscopic quantum emitters,” *Nature Physics*, vol. 7, pp. 215–218, mar 2011.

**Supplementary Material for:**  
**Shaping Polaritons to Reshape Selection Rules**

Francisco Machado<sup>\*1</sup>, Nicholas Rivera<sup>\*1</sup>, Hrvoje Buljan<sup>2</sup>, Marin Soljačić<sup>1</sup>, Ido Kaminer<sup>1</sup>

<sup>1</sup>*Department of Physics, Massachusetts Institute of Technology, Cambridge, MA 02139, USA*

<sup>2</sup>*Department of Physics, University of Zagreb, Zagreb 10000, Croatia.*

## VI. INTRODUCTION TO SUPPLEMENTARY MATERIAL

In this Supplementary Material we derive expressions for rates of transitions in which an atom absorbs (or emits) a polariton with orbital angular momentum. We will focus on the particular case of 2D plasmons described by a local Drude model and hyperbolic surface phonon polaritons in uniaxial hBN. However, we present our results in a form that allows for straightforward extension not only to other conductivity models for 2D plasmonic materials but also to other surface polaritons such as surface exciton polaritons. We begin by constructing the classical vortex modes for polaritons that are highly confined. Then we develop quantized field operators in this basis of modes with definite orbital angular momentum and we use these operators to compute transition rates at first and second order in perturbation theory.

## VII. APPENDIX 1: CONSTRUCTION OF CLASSICAL POLARITONIC VORTEX MODES IN (AN)ISOTROPIC DIELECTRICS

In this section we describe classical surface polariton plane-wave modes for the case of a thin metallic film surrounded by dielectric. Through superposition of these planar modes we build vortex modes labeled by the winding number of the phase. Having described the vortex modes, we prove their orthogonality and show how translated vortex modes can be resolved in a superposition of non-translated (centered) vortex modes. We then develop a simpler formalism for constructing vortex modes, one that works when the vortex modes are highly sub-wavelength (i.e., when the modes are nearly longitudinal (curl-free) and thus well-described by a scalar electric potential).

### A. General Construction

Surface polariton modes generically correspond to excitations in solids which are coupled to electromagnetic modes highly confined to the interface of the material. Of particular interest are surface plasmon polaritons (SPP) and surface phonon polaritons (SPhP), where the solid excitation corresponds to a plasmon or phonon respectively. But other surface polaritons exist in nature, such as surface exciton polaritons in semiconductors like ZnO, and CuCl. The electromagnetic modes associated with these surface polaritons can be obtained by solving Maxwell's equations with the particular dielectric function (which may be spatially non-local) of the polaritonic material. For a

thin film (quasi-2D) geometry with surrounding dielectrics (as in Figure (6) of the main text), the planar SP(h)P mode is given by [1]:

$$\mathbf{A}_{\mathbf{q},K} = \frac{A_0}{\sqrt{q^2 + K^2}} (K\hat{q} + iq\hat{z}) e^{-zK} e^{i(\mathbf{q}\cdot\boldsymbol{\rho} - \omega t)} \xrightarrow{\text{electrostatic limit}} \mathbf{A}_{\mathbf{q}} = \frac{A_0}{\sqrt{2}} (\hat{q} + i\hat{z}) e^{-qz} e^{i(\mathbf{q}\cdot\boldsymbol{\rho} - \omega t)} \quad (z > 0), \quad (6)$$

where  $\mathbf{q}$  is the in-plane momentum,  $1/K$  is the out of plane decay length,  $z$  is the out of plane coordinate,  $\boldsymbol{\rho}$  is the in-plane position,  $\omega$  is the frequency of the mode,  $A_0$  is the amplitude of the mode and hats represent unit vectors. Within the electrostatic limit,  $q \gg \omega/c$ , the inverse decay length of the mode equals the in-plane momentum,  $K \approx q$ , enabling the approximation in Eq. (1).

Having described the plane-wave surface polariton mode, we now build the vortex polariton modes as a superposition of surface plane-wave modes whose superposition coefficients are phases ( $e^{im\alpha}$ ) proportional to the angle ( $\alpha$ ) of the plane-wave mode. In order for the mode to be well defined, as one goes around the vortex center, the phase of the mode must change by  $2\pi m$  for  $m \in \mathbb{Z}$ . The value of  $m$  corresponds to the winding number of the phase around the vortex center and determines the angular momentum  $\hbar m$  of the mode. When we discuss selection rules for electronic transitions involving the emission and absorption of vortex polaritons, we will be in a position to justify the interpretation of  $\hbar m$  as angular momentum. The vortex mode is given by:

$$\mathbf{A}_{\mathbf{q},m} = \frac{1}{2\pi} \int_0^{2\pi} d\alpha \frac{A_0}{\sqrt{2}} e^{i(\mathbf{q}\cdot\boldsymbol{\rho} - \omega t)} e^{i\alpha m} \begin{cases} (\hat{q} + i\hat{z}) e^{-qz} & (z > 0) \\ \hat{q} & (z = 0) \\ (\hat{q} - i\hat{z}) e^{qz} & (z < 0), \end{cases} \quad (7)$$

where  $\alpha$  is angle between  $\mathbf{q}$  and some reference direction, set to be  $\hat{x}$  without loss of generality. Let  $\phi$  be the angle between  $\boldsymbol{\rho}$  and  $\hat{x}$ . Using the Jacobi-Anger expansion [2] and the orthogonality of complex exponentials, we obtain, for  $z > 0$ :

$$\begin{aligned} \mathbf{A}_{\mathbf{q},m} &= \frac{A_0}{2\sqrt{2}\pi} e^{-qz} \int_0^{2\pi} d\alpha (\cos(\alpha)\hat{x} + \sin(\alpha)\hat{y} + i\hat{z}) e^{iq\rho \cos(\alpha-\phi)} e^{i\alpha m} \\ &= \frac{A_0}{4\sqrt{2}\pi} e^{-qz} \int d\alpha ((e^{i\alpha} + e^{-i\alpha})\hat{x} - i(e^{i\alpha} - e^{-i\alpha})\hat{y} + i2\hat{z}) \sum_{n=-\infty}^{\infty} i^n J_n(q\rho) e^{in(\alpha-\phi)} e^{i\alpha m} \\ &= \frac{A_0}{2\sqrt{2}} e^{-qz} e^{im\phi} i^{m+1} \left\{ (\hat{x} - i\hat{y}) J_{m+1}(q\rho) e^{i\phi} - (\hat{x} + i\hat{y}) J_{m-1}(q\rho) e^{-i\phi} + \hat{z} 2J_m(q\rho) \right\} \end{aligned}$$

which implies more generally that

$$\mathbf{A}_{q,m} = e^{-q|z|} \frac{A_0}{2\sqrt{2}} e^{im\phi} i^{m+1} \left( \hat{\rho} [J_{m+1}(q\rho) - J_{m-1}(q\rho)] - i\hat{\phi} \frac{2mJ_m(q\rho)}{q\rho} + \begin{cases} \hat{z} 2J_m(q\rho) & (z > 0) \\ 0 & (z = 0) \\ -\hat{z} 2J_m(q\rho) & (z < 0) \end{cases} \right). \quad (8)$$

## B. Energy and Orthogonality of Vortex Modes

Consider the following inner product between two modes (which is proportional to the time-averaged energy density of the mode):

$$\langle \mathbf{A}_{q,n}, \mathbf{A}_{k,m} \rangle = \int d\mathbf{r} \frac{1}{2\omega} \frac{d(\epsilon_r \omega^2)}{d\omega} \mathbf{A}_{q,n}^*(\mathbf{r}) \mathbf{A}_{k,m}(\mathbf{r}). \quad (9)$$

For the purposes of this work we consider the substrate and superstrate to be negligibly dispersive in the frequency range of interest ( $\frac{\partial \epsilon}{\partial \omega} \ll \frac{\epsilon}{\omega}$ ). For the case of 2D plasmons, we consider the Drude model for the dielectric response of a metal, given by:

$$\epsilon_{r,metal} = 1 - \frac{\omega_p^2}{\omega^2}, \quad (10)$$

where  $\omega_p$  is the plasmon frequency of the metal. For the integration of the thin metallic film volume, we take a finite width slab and take the limit as the thickness  $d$  goes to zero. The dielectric function can then be written as:

$$\epsilon_{r,film} = \left(1 - \frac{\omega_p^2}{\omega^2}\right) \theta(d/2 - |z|) \xrightarrow{d \rightarrow 0} \epsilon_{r,film} = \left(1 - \frac{\omega_p^2}{\omega^2}\right) d\delta(z),$$

where  $\theta(x)$  is a step function. The derivative term will cancel the  $\omega_p^2/\omega^2$  terms, while the first term is zero in the limit  $d \rightarrow 0$ . The inner product then simplifies to (for the Drude plasmons with high confinement):

$$\langle \mathbf{A}_{q,n}, \mathbf{A}_{k,m} \rangle = 2\bar{\epsilon}_r \int_{z>0} d\mathbf{r} \mathbf{A}_{q,n}^*(\mathbf{r}) \mathbf{A}_{k,m}(\mathbf{r}),$$

where  $\bar{\epsilon}_r$  is the average dielectric surrounding the metallic film. By definition this integral is:

$$\begin{aligned} \langle \mathbf{A}_{q,n}, \mathbf{A}_{k,m} \rangle &= \bar{\epsilon}_r \frac{A_0^2}{2} \int_0^\infty dz \int_0^\infty d\rho \rho \int_0^{2\pi} d\phi e^{-z(q+k)} e^{i(m-n)\phi} \times \\ &\quad \times [J_{m+1}(k\rho)J_{n+1}(q\rho) + J_{m-1}(k\rho)J_{n-1}(q\rho) + 2J_m(k\rho)J_n(q\rho)] \end{aligned}$$

Since the  $\phi$  integration imposes  $m = n$ , the cosines differ only by their argument  $k\rho$  or  $q\rho$ . Using the orthogonality of Bessel functions, i.e.,  $\int d\rho \rho J_m(k\rho)J_m(q\rho) = \frac{1}{k}\delta(k - q)$ , we see that the inner product vanishes for  $k \neq q$ , so the modes are orthogonal. For  $k = q$ , we can evaluate the inner product (proportional to " $\delta(0)$ ") by setting the upper limit of the radial integral to a normalization length (also often called a quantization length),  $L$ , much larger than any length scale associated with the plasmonic vortex. Any result we will derive will be independent of  $L$ . Setting the upper limit of the integral to  $L$ , we see that the inner product for  $k = q$  is simply  $\frac{L}{\pi q}$ .

### 1. Angular Momentum Representation of Displaced Vortices

To define a vortex mode displaced from our coordinate center by  $\mathbf{D}$  we consider the translation of Equation (7) by  $\mathbf{D}$  (setting  $\boldsymbol{\rho}$  to  $\boldsymbol{\rho} - \mathbf{D}$ ):

$$\mathbf{A}_{q,m}^{\mathbf{D}} = \frac{1}{2\pi} \int d\alpha \frac{A_0}{\sqrt{2}} (\hat{q} + i\hat{z}) e^{-qz} e^{i(\mathbf{q} \cdot \boldsymbol{\rho} - \omega t)} e^{-i\mathbf{q} \cdot \mathbf{D}} e^{i\alpha m} \quad (z > 0). \quad (11)$$

Applying the Jacobi-Anger relation to the term  $e^{-i\mathbf{q} \cdot \mathbf{D}}$  one obtains:

$$e^{-i\mathbf{q} \cdot \mathbf{D}} = e^{-iqD \cos(\alpha - \phi_0)} = \sum_{n=-\infty}^{\infty} (-i)^n J_n(qD) e^{in(\alpha - \phi_0)}, \quad (12)$$

where  $\phi_0$  is the angle between  $\mathbf{D}$  and the chosen reference direction ( $\hat{x}$  here). The displaced vortex mode can then be easily written as:

$$\begin{aligned} \mathbf{A}_{q,m}^{\mathbf{D}} &= \sum_{n=-\infty}^{\infty} (-i)^n J_n(qD) e^{-in\phi_0} \frac{1}{2\pi} \int d\alpha \frac{A_0}{\sqrt{2}} (\hat{q} + i\hat{z}) e^{-qz} e^{i(\mathbf{q} \cdot \boldsymbol{\rho} - \omega t)} e^{i\alpha(m+n)} \quad , \quad (z > 0) \\ &= \sum_{n=-\infty}^{\infty} (-i)^{n-m} J_{n-m}(qD) e^{-i(n-m)\phi_0} \mathbf{A}_{q,n}. \end{aligned} \quad (13)$$

The displaced vortex can thus be written as a simple superposition of vortex modes centered around the coordinate system. This fact enables us to reduce the displaced vortex mode case to a superposition over centered vortex modes, whose computation and understanding is much easier due to the symmetry of the mode.

### C. Quasi-Electrostatic Limit: Scalar Potential Formalism

We now discuss an alternative and simpler method for computing the vortices which applies for fields which are approximately described by the gradient of a scalar potential (i.e., approximately

longitudinal) [15]. As can be seen from the plane-wave polariton modes in the electrostatic limit, they can indeed be written as the gradient of a scalar potential. By the linearity of derivatives, the vortex modes constructed from these plane-wave modes can also be expressed as gradients of scalar-potential vortex modes. We now focus on constructing these vortices for *any* uniaxial or isotropic medium. We include the possibility of uniaxial anisotropy due to the recent interest in the phonon-polaritons of hBN. To find the modes, we merely solve the Laplace equation subject to appropriate boundary conditions. The Laplace equations in each region read (using repeated index notation):

$$\partial_i \epsilon_{ij} \partial_j \phi = 0.$$

The translational invariance in-plane admits scalar potential solutions of the form  $Z(z)e^{i\mathbf{q}\cdot\boldsymbol{\rho}}$ . Taking the optical axis of a uniaxial crystal to be perpendicular to the slab illustrated in Figure (6) of the main text, the dielectric function of such a uniaxial crystal can be written as  $\epsilon(\omega) = \text{diag}(\epsilon_{\perp}(\omega), \epsilon_{\perp}(\omega), \epsilon_{\parallel}(\omega))$ . In that case, the Laplace equation becomes:

$$-\frac{\epsilon_{\perp}}{\epsilon_{\parallel}}q^2Z + \frac{d^2Z}{dz^2} = 0 \implies \frac{d^2Z}{dz^2} = r^2q^2Z,$$

where the anisotropy ratio,  $r$  is defined as  $\sqrt{\frac{\epsilon_{\perp}}{\epsilon_{\parallel}}}$ . The scalar potential vortex mode is thus defined as:

$$\phi_{q,m} \equiv \frac{1}{\sqrt{2}q} N_{q,m} Z_q(z) \int_0^{2\pi} \frac{d\alpha}{2\pi} e^{i\alpha m + i q \rho \cos(\alpha - \phi)}, \quad (14)$$

where  $N_{q,m}$  is a normalization constant to be specified during quantization and where we have used the fact that due to the rotational symmetry in-plane,  $Z_q(z)$  is independent of the angle that the wavevector makes to the reference direction. Via the Jacobi-Anger expansion, this previous expression becomes

$$\phi_{q,m} = \frac{1}{\sqrt{2}q} i^m N_{q,m} Z_q(z) J_m(q\rho) e^{im\phi}. \quad (15)$$

The electric field (in either  $\phi = 0$  gauge or Coulomb gauge) and vector potential modes (in the Coulomb gauge) must be proportional to the gradient of this scalar potential mode in the electrostatic limit. The electric field vortices are therefore:

$$\mathbf{E}_{q,m} = -\nabla \phi_{q,m} = -\frac{1}{\sqrt{2}q} i^m N_{q,m} e^{im\phi} Z_q \left[ \frac{\partial J_m(q\rho)}{\partial \rho} \hat{\rho} + \frac{im}{\rho} J_m(q\rho) \hat{\phi} + \frac{1}{Z_q} \frac{dZ_q}{dz} J_m(q\rho) \hat{z} \right].$$



The vector potentials (in the  $\phi = 0$  gauge) are just  $\frac{1}{i\omega}\mathbf{E}$ . Using derivative relations for Bessel functions, the above equation can be seen to be:

$$\mathbf{E}_{q,m} = \frac{1}{2\sqrt{2}} i^m N_{q,m} e^{im\phi} Z_q \left[ [J_{m+1}(q\rho) - J_{m-1}(q\rho)] \hat{\rho} - \frac{2im}{q\rho} J_m(q\rho) \hat{\phi} - 2 \frac{1}{qZ_q} \frac{dZ_q}{dz} J_m(q\rho) \hat{z} \right]. \quad (16)$$

We pause to note that taking  $Z_q(z) \sim e^{-q|z|}$  for graphene yields a field proportional to Equation (3), confirming that the vortices can also be derived from a scalar potential vortex – no surprise given the high confinement of the modes. Therefore, this approach very straightforwardly allows for the calculation of quasielectrostatic vortices in any 2D-translationally-invariant photonic system. One simply needs the appropriate  $Z_q(z)$ . To deal with isotropic systems, one need simply set  $\epsilon_{\perp}$  to  $\epsilon_{\parallel}$  from the beginning.

We conclude this section by noting that the electrostatic limit leads to remarkably simple expressions, despite the anisotropy of the system. It is important that we presented both a formalism which did not crucially rely on the electrostatic potentials (computing the vector potential of the mode, accounting for retardation), and a formalism which takes the electrostatic limit as its primary assumption. Obviously, the latter formalism is much simpler computationally. That said, the first formalism can be quite useful for plasmons which are not so strongly confined, as in the case of plasmons on top of a thick film of noble metal like silver or gold. The latter formalism is also useful for OAM carrying whispering gallery modes in micro-ring resonators. For problems in which relatively large emitters like quantum dots are interfaced with these electromagnetic modes, an approach ignoring retardation effects would be questionable, and for this reason, we have provided a formalism by which to understand the interaction between matter and vortices, even outside of the electrostatic limit.

## VIII. APPENDIX 2: CONSTRUCTION OF QUANTUM FIELDS FOR POLARITONIC VORTICES IN THE ANGULAR MOMENTUM BASIS

### A. Field Operators

Here, we derive the quantized electromagnetic field operators needed to describe interactions between electrons and polaritons. Since the main interest of our paper is vortex-enabled light-matter interactions, we will write the field operators in the angular momentum basis. Moreover, since the most interesting situations arise when the electromagnetic fields are approximately longitudinal,

we will focus on those in this section. The extension to fields which are not quasi-electrostatic is straightforward. In the first part, we will derive the form of the vector potential operator in the  $\phi = 0$  gauge, whose use can be extended to non-quasistatic vortices. Then we will present (just like in the last section) an alternative and simpler method of calculation via scalar potentials which can be used in the Coulomb gauge.

### 1. Vector Potential in the $\phi = 0$ Gauge

We will now find the normalization of these modes that makes them suitable for QED calculations. The prescription for writing down field operators such as the vector potential operator is to write it as [3]:

$$\mathbf{A} = \sum_{q,m} \sqrt{\frac{\hbar}{2\epsilon_0\omega_{q,m}}} (a_{q,m} \mathbf{F}_{q,m} + h.c), \quad (17)$$

where the  $\mathbf{F}_{q,m}$  are proportional to  $\mathbf{E}_{q,m}$  but normalized such that  $\int \frac{1}{2\omega} \mathbf{F}_{q,m}^* \cdot \frac{d(\epsilon\omega^2)}{d\omega} \cdot \mathbf{F}_{q,m} = 1$ . The double dot product is present because of the regions of anisotropic dielectric. The energy integral takes the form:

$$\frac{1}{2\omega} \int dz d\phi d\rho \rho \frac{d(\epsilon_{\perp}\omega^2)}{d\omega} (|F_{q,m}^x|^2 + |F_{q,m}^y|^2) + \frac{d(\epsilon_{||}\omega^2)}{d\omega} |F_{q,m}^z|^2.$$

Taking  $\mathbf{F}_{q,m}$  to be given by Equation (12) and performing the azimuthal integral first yields a factor of  $2\pi$ . Performing the radial integral, making use of the orthogonality of Bessel functions yields (via the same arguments as those used when we computed the energy of graphene vortices in Sec. 2.2):

$$\frac{2|N_{q,m}|^2 L \bar{\epsilon}_r \xi_q}{q^2},$$

where  $\xi_q$  is dimensionless and given by:

$$\xi_q = \frac{q}{4\omega\bar{\epsilon}_r} \int dz \left[ \frac{d(\epsilon_{\perp}\omega^2)}{d\omega} |Z|^2 + \frac{d(\epsilon_{||}\omega^2)}{d\omega} \frac{1}{q^2} \left| \frac{dZ}{dz} \right|^2 \right]. \quad (18)$$

We therefore see that the vector potential is given by:

$$\mathbf{A} = \sum_{q,m} \sqrt{\frac{\hbar q^2}{4\epsilon_0\bar{\epsilon}_r L \omega_{q,m} \xi_q}} (a_{q,m} \mathbf{F}_{q,m} + h.c), \quad (19)$$

where

$$\mathbf{F}_{q,m} = \frac{1}{2\sqrt{2}} i^m e^{im\phi} Z(z) \left( [J_{m+1}(q\rho) - J_{m-1}(q\rho)] \hat{\rho} - \frac{2im}{q\rho} J_m(q\rho) \hat{\phi} - 2 \frac{1}{qZ_q} \frac{dZ_q}{dz} J_m(q\rho) \hat{z} \right). \quad (20)$$

In the region ( $z > d/2$ ), we have that  $Z_q(z)$  is just  $e^{-qz}$ . Therefore, the expression for  $\mathbf{F}_{q,m}$  exactly matches Equation (3). We have defined  $\xi_q$  in order to make the field operators for other polaritons strongly resemble those field operators for graphene. In fact, for graphene (or any 2D plasmonic material with Drude dispersion),  $\xi_q = 1$ . The electric field operator is derived from the vector potential in a gauge where the scalar potential is zero via  $\mathbf{E} = i\omega\mathbf{A}(\omega)$  (this means that the h.c. term picks up a relative minus sign since it is counter-rotating relative to the first term in the Heisenberg representation of the field operator).

### 2. Scalar Potential in the Coulomb Gauge: $\nabla \cdot \mathbf{A} = 0$

Changing to Coulomb gauge and using the electrostatic limit, the vector potential vanishes everywhere. Now, all the dynamics are generated by a scalar potential. Using the potentials in Equation (11) with the derived normalization, the scalar potential operator can be written:

$$\phi = \sum_{q,m} \sqrt{\frac{\hbar\omega}{4\epsilon_0\bar{\epsilon}_r\xi_q L}} (a_{q,m}U_{q,m} + h.c.), \quad (21)$$

where

$$U_{q,m} = \frac{1}{\sqrt{2}} i^m Z_q(z) J_m(q\rho) e^{im\phi}. \quad (22)$$

### 3. $\xi_q$ for Different Materials

Our findings apply to all uniaxial media whose surface polaritons are well described by longitudinal electric fields. The difference between each material is contained in the  $\xi_q$  factor and the ratio  $c/v_g$ . It applies to plasmons in graphene, to 2D plasmons in metallic monolayers, to phonon-polaritons in hBN or SiC [4, 5], to the acoustic plasmons in gated graphene [6], to surface exciton polaritons like in MoS<sub>2</sub> [7] and in newly discovered phase-change materials [8], and could, with straightforward extension of the formalism, apply to anisotropic plasmons in black phosphorus [9].  $\xi_q$  was defined for graphene such that  $\xi_q(\text{graphene}) = 1$ . The reason for this is that the rates of various electronic transitions in the vicinity of graphene take very simple analytic forms [10] (simpler than all of the other materials we mentioned in the text). That makes it easy to understand the order of magnitude of transitions in other materials by making graphene the reference material.

Of course, all materials are different, and material-specific and emitter-specific challenges arise when interfacing particular emitters with particular materials. Because of this it is important to formulate our theory in a way that makes explicit that similar results hold for all the possible platforms for realizing the predictions of the theory. It makes explicit the fact that from the perspective of photonics and transition rates, all of these above-mentioned materials are similar. Thus, we hope that the unity of the treatment of different polaritonic materials will serve to provide a platter of options for realizing the predictions of the theory.

In the rest of this section, we discuss explicitly (i.e., with numbers) the case of hyperbolic polaritons in a slab of hexagonal boron nitride of thickness  $d$ . The electric field plane-wave modes can be shown to be:

$$\mathbf{E}_{q,m} = \frac{E_0}{i\omega\epsilon_0} \epsilon_r^{-1}(z) \nabla \times \hat{q}_\perp \begin{cases} e^{-qz} & (z > 0) \\ \frac{e^{ikd} \epsilon_\perp q (\epsilon_s k - i \epsilon_\perp q)}{2k(-\epsilon_\perp q \cos(kd) + \epsilon_s k \sin(kd))} e^{ikz} + \frac{\epsilon_\perp q (-i \epsilon_s k + \epsilon_\perp q)}{k(\epsilon_s k + i \epsilon_\perp q + e^{2ikd}(-\epsilon_s k + i \epsilon_\perp q))} e^{-ikz} & (-d < z < 0) \\ \frac{e^{qd} q \epsilon_\perp \epsilon_s}{-\epsilon_\perp q \cos(kd) + \epsilon_s k \sin(kd)} e^{qz}, & (z < -d) \end{cases} \quad (23)$$

where  $\epsilon_r$  is the relative permittivity of the hBN which is given by  $\text{diag}(\epsilon_\perp, \epsilon_\perp, \epsilon_\parallel)$ ,  $\epsilon_s$  is the relative permittivity of the substrate,  $q$  is the wavevector,  $k \equiv q\sqrt{r}$ ,  $r = \left| \frac{\epsilon_\perp}{\epsilon_\parallel} \right|$ ,  $\hat{q}_\perp$  is a unit vector along the in-plane direction perpendicular to the wavevector, and  $E_0$  is a normalization constant. The dispersion satisfies the following implicit equation:

$$\tan(kd) = \frac{1 + \epsilon_s}{\frac{\epsilon_s \sqrt{r}}{\epsilon_\perp} - \frac{\epsilon_\perp}{\sqrt{r}}}. \quad (24)$$

These two pieces of information suffice to compute the confinement, group velocity, and  $\xi_q$  factors for hBN. In Figure (7), we show how the factor  $\xi_q v_g$  compares between hBN and graphene plasmons for hBN films of different thicknesses. We perform the computation in the upper Reststrahlen band. The only difference in emission and absorption rates of single vortex polaritons comes from these factors and yet we see that the two factors are within the same order of magnitude, making it clear and explicit that hBN vortices can be used to tailor selection rules in atomic systems.

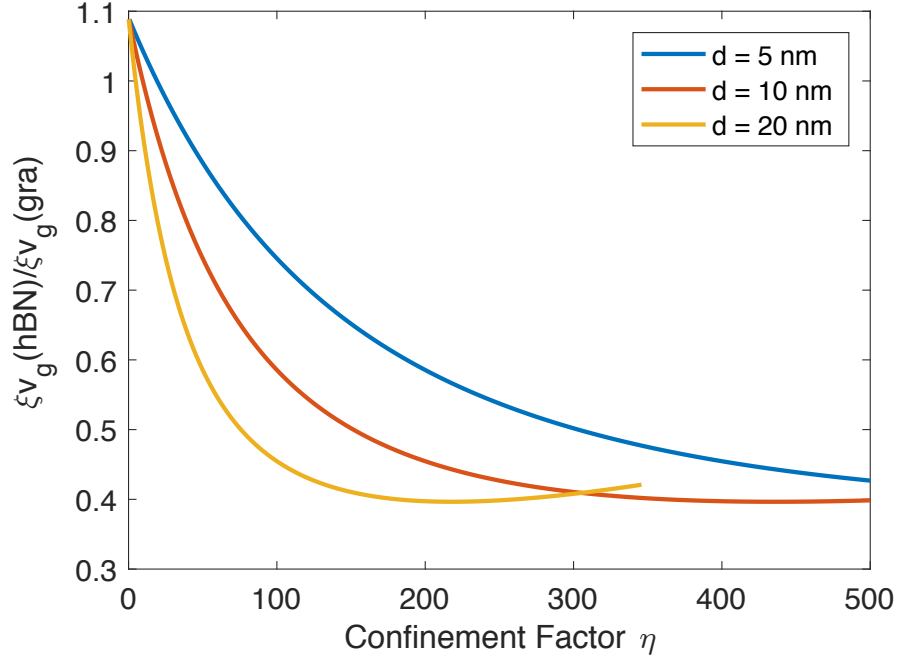


FIG. 6: Comparison of the product  $\xi_q v_g$  between hBN and graphene for hBN slabs of thicknesses 5, 10, and 20 nm. The comparison is done as a function of confinement in order to achieve a direct comparison between the strengths of light-matter interactions at fixed confinement factor. The plot is terminated at a maximum confinement of 500 (a polariton wavelength of about 10 nm), although the theory predicts potentially even higher confinements for the 5 and 10 nm thick hBN near the very edge of the Reststrahlen band. The yellow curve terminates at a confinement of 300 because the maximum frequency for which the confinement is computed is  $1600 \text{ cm}^{-1}$ .

### IX. APPENDIX 3: ANGULAR MOMENTUM AND LIGHT-MATTER INTERACTIONS

#### A. First-Order Processes

The transition rate for the absorption is calculated using Fermi's Golden Rule (for radiation with a frequency spectrum much broader than the linewidth of the excited state):

$$\Gamma = \frac{2\pi}{\hbar} |\langle \phi_f, n-1 | H_{int} | \phi_i, n \rangle|^2 \rho_m(\hbar\omega) \quad (25)$$

where  $\phi_i$  ( $\phi_f$ ) is the electronic initial (final) state,  $n$  corresponds to the number of photons in our

mode of interest,  $\rho_m(\hbar\omega)$  corresponds to the density of vortex modes at each angular momentum  $\hbar m$  [16].  $H_{int}$  is the interaction Hamiltonian  $\frac{e}{2m}(\mathbf{p} \cdot \mathbf{A} + \mathbf{A} \cdot \mathbf{p}) + \frac{e^2}{2m}\mathbf{A}^2$  in the  $\phi = 0$  gauge and  $e\phi$  in the Coulomb gauge. To compute  $\rho_m(\hbar\omega)$  consider a perfectly conducting cylinder of extremely large radius (quantization length)  $L$  surrounding the vortex mode (for example, take  $L = 1$  m). At  $L$ , the non-radial components of the field must vanish. Using the large distance asymptotic form of the Bessel functions, the  $q$  spacing of allowed states is given by  $\pi/L$ . The density of states is then given by:

$$\rho_m(\hbar\omega_0) = \frac{L}{\pi} \int dq \delta(\hbar\omega_0 - \hbar\omega) = \frac{L}{\pi\hbar} \frac{1}{|\mathbf{v}_q|}, \quad (26)$$

where  $\mathbf{v}_q$  is the group velocity  $\frac{d\omega}{dk}$  of the mode at energy  $\omega_0$ . Note that by definition, the  $q$  in the vortex mode is  $|\mathbf{q}|$  and is therefore positive. In the case of SPP, the dispersion relation is approximately given by [1] (where  $\beta$  is a proportionality constant which will appear nowhere in the final answers below) :

$$q = \beta\omega^2 \quad \Rightarrow \quad \frac{dq}{d\omega} = 2\beta\omega \quad \Rightarrow \quad v_q = \frac{1}{2\beta\omega} = \frac{c}{2\eta},$$

where  $\eta$  is the confinement factor  $\frac{qc}{\omega}$ , which is the ratio of photon and polariton wavelengths at the same frequency. The absorption rate of the system is given by (taking the vector potential interaction Hamiltonian):

$$\begin{aligned} \Gamma &= \frac{2\pi}{\hbar^2} \frac{L}{\pi} \frac{2\eta}{c} \frac{e^2}{m^2} \frac{n\hbar q^2}{4\bar{\epsilon}_r\epsilon_0 L\omega_{q,m}\xi_q} |\langle\phi_f, n-1|\mathbf{F}_{q,m} \cdot \hat{p}|\phi_i, n\rangle|^2 \\ &= \frac{4\pi e^2}{4\pi\epsilon_0\hbar c} \frac{n\eta^3\omega}{\bar{\epsilon}_r\xi_q} \frac{|\langle\phi_f, n-1|\mathbf{F}_{q,m} \cdot \hat{p}|\phi_i, n\rangle|^2}{m^2 c^2} \\ &= \frac{4\pi n\alpha\eta^3\omega}{\bar{\epsilon}_r\xi_q} \frac{|\langle\phi_f|\mathbf{F}_{q,m} \cdot \hat{p}|\phi_i\rangle|^2}{m^2 c^2}. \end{aligned} \quad (27)$$

The photon number  $n$  is derived by applying the correspondence principle to a hypothetically monochromatic radiation field (relative to its central frequency, but still much broader than the atomic linewidth due to spontaneous emission or collisions). This follows the treatment in [11]. Consider a classical field with energy density per unit frequency  $\frac{dU}{d\omega}$ . This should just be equal to the mean photon number at frequency  $\omega$  ( $\langle n(\omega) \rangle$ ) times  $\hbar\omega$  times the density of states  $\rho(\omega)$ . In that case, the mean photon number is simply  $\frac{1}{\rho\hbar\omega} \frac{dU}{d\omega}$ , where  $U$  is the energy of an approximately single mode with the field amplitude of the classical field in the experiment of interest[17].

We also point out here what happens if for some reason, the radiation is narrower than the linewidth of the excited atomic state (either due to radiation or other broadening mechanisms).

We'll consider only the case of radiative broadening. In that case, the fact that the excited state is actually a continuum of width  $\Gamma_d$  is relevant (where  $\Gamma_d$  is the decay rate of the excited atomic state). In such a case, Fermi's Golden Rule would give that the decay rate is (on resonance) roughly equal to  $\frac{2\pi}{\hbar^2\Gamma_d}|\frac{e}{m}\mathbf{A}\cdot\mathbf{p}|_{eg}^2$ , where  $\mathbf{A}$  is the vector potential amplitude of the approximately monochromatic (and semiclassical) radiation [12]. Nevertheless, we see that the same matrix elements appear as in the broadband case, meaning that angular momentum conservation still appears in the transition rates. Therefore, regardless of whether the vortex (of fixed angular momentum) is broadband or monochromatic, it can still be used to control electronic transitions.

### 1. Long-Wavelength Approximation

To check the consistency of our result, we compute the transition rates of dipoles associated with hydrogen transitions near a graphene layer ( $\xi_q = 1$ ) and compare the results with the literature [13]. In the case of a z-dipole transition,  $m_i = m_f = 0$ , so the only contribution to the transition rate is the 0-th order vortex mode. As a result  $\langle\phi_f|\hat{x}|\phi_i\rangle = \langle\phi_f|\hat{y}|\phi_i\rangle = 0$ . Using the relation  $\hat{p} = -\frac{i\hbar}{m}[\hat{x}, H_{ele}]$ , we can show that  $-i\omega\langle\phi_f|\hat{x}_j|\phi_i\rangle = \langle\phi_f|\hat{p}_j|\phi_i\rangle$ , where  $j$  labels the direction.

Considering a vortex mode whose wavelength is much larger than the atomic radius, the transition rate is only dependent on the field at the position of the atom.

$$\begin{aligned}\Gamma_{\text{z-dip}} &= \frac{4\pi n\alpha\eta^3\omega}{\bar{\epsilon}_r} \frac{|\mathbf{F}_{0,q}^j(0,0,z_0)\langle\phi_f|\hat{p}_j|\phi_i\rangle|^2}{m^2c^2} = \frac{4\pi n\alpha\eta^3\omega}{\bar{\epsilon}_r} \frac{e^{-2q|z_0|}}{2} J_0(0)^2 m^2\omega^2 |\langle\phi_f|\hat{z}|\phi_i\rangle|^2 \\ &= \frac{2\pi n\alpha\eta^3\omega^3}{\bar{\epsilon}_r} e^{-2q|z_0|} |\langle\phi_f|\hat{z}|\phi_i\rangle|^2.\end{aligned}\quad (28)$$

The corresponding transition due to plane wave modes in vacuum is given by:

$$\Gamma_{\text{free}} = \frac{4n\alpha\omega^3}{3c^2} |\langle\phi_f|\hat{z}|\phi_i\rangle|^2.$$

The presence of the polariton supporting graphene layers leads to an enhancement (Purcell factor) of:

$$\frac{\Gamma_{\text{z-dip}}}{\Gamma_{\text{free}}} = \frac{3\pi}{2\bar{\epsilon}_r} \eta^3 e^{-2q|z_0|}.\quad (29)$$

Next we consider the decay rate for a dipole polarized in the  $x$ -direction. We perform this calculation in the Coulomb gauge since it is easier here. Decay rates of course cannot depend on the choice of gauge [18]. Such a dipole can be seen as a superposition of an  $m = 1$  and an  $m = -1$  dipole (i.e., a sum of oppositely oriented but circularly polarized dipoles). This means that the

decay rate will have contributions from emission of an  $m = 1$  vortex and an  $m = -1$  vortex. Since the dipole is  $x$ -polarized, only the  $\cos \phi$  part of  $e^{i\phi}$  or  $e^{-i\phi}$  will contribute to the matrix elements. The total decay rate is therefore:

$$\Gamma_{x-dip} = 2 \times \frac{4\pi n \alpha \eta^3 \omega^3}{\bar{\epsilon}_r} \left| \int d\mathbf{r} \psi_g^* J_1(q\rho) Z_q(z) \cos \phi \psi_e \right|^2. \quad (30)$$

Performing an expansion of the  $J_1(q\rho) Z_q(z)$  term about the position of the atom  $(0, 0, z_0)$  and using the fact that  $J_1(x) \approx x/2$  for small  $x$ , we have that the decay rate is:

$$\Gamma_{x-dip} = \frac{1}{2} \times \frac{4\pi n \alpha \eta^3 \omega^3}{\bar{\epsilon}_r} |Z_q(z_0)|^2 \left| \int d\mathbf{r} \psi_g^* r \sin \theta \cos \phi \psi_e \right|^2. \quad (31)$$

Setting  $Z(z_0) = e^{-qz_0}$  and comparing the resulting expression to  $\Gamma_{z-dip}$ , we see that the emission/absorption from an  $x$ -polarized dipole is half as much as from a  $z$ -polarized dipole with the same dipole moment. The same argument will show that for a  $y$ -polarized dipole, the emission is half as much as from a  $z$ -polarized dipole with the same dipole moment. These decay rates for  $z$ - and in-plane polarized dipoles match the results obtained in [13] for the decay rates of emitters into graphene plasmons.

## 2. Absorption rates of $m_{vortex} = 5$ $SP(h)P$ mode with starting state $(5, 0, 0)$

Here, we provide the results of numerical calculations of absorption rates (normalized by the number of photons) for transitions between principal quantum number 5 and 6 in hydrogen. We do this here to provide more examples of the order of magnitudes of transition rates in the hydrogen atom as a function of multipolarity,  $z$ -projected angular momentum change, and displacement of the atom from the vortex center.



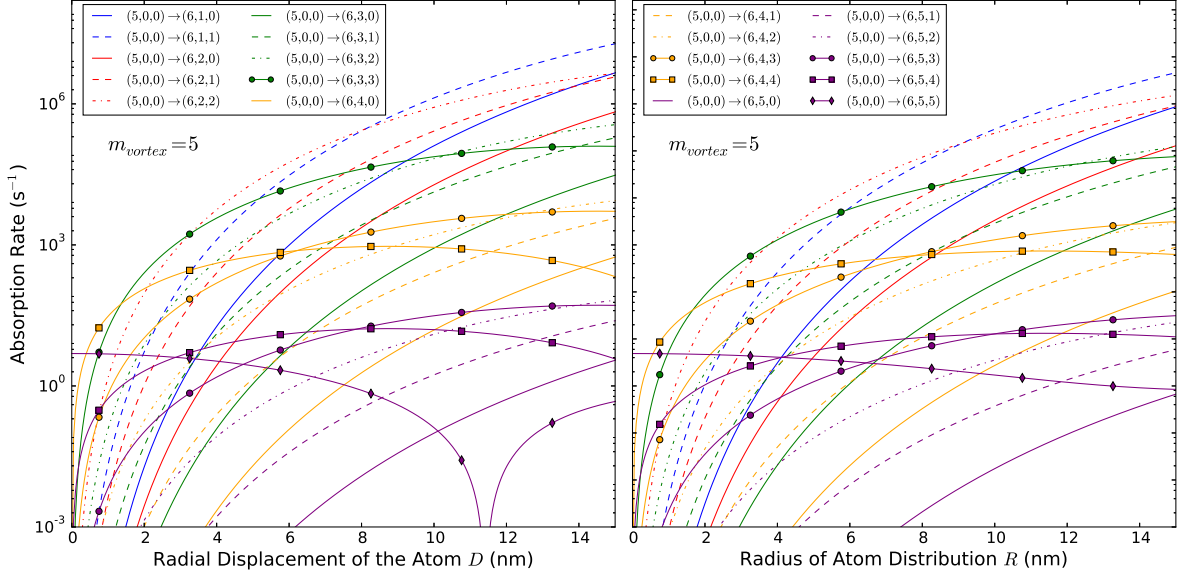


FIG. 7: Single photon absorption rate of a vortex mode with OAM of  $5\hbar$  between the state  $(5,0,0)$  and all states in the family  $(6,l,m)$  with  $z_0 = 20$  nm. This plot is based on Figure (4) in the main text but includes all possible transitions to states in  $(6,l,m)$ . By including non-dominant transitions, the competition between the baseline absorption rate and the Bessel function coefficient becomes more visible, even between transitions to the same value of  $l$  (same color). Moreover, for transitions to the same  $m$  (same linestyle), they are exactly proportional to one another (vertical translations in this log-plot), as their Bessel function coefficient is the same, and only the baseline absorption rate varies.

## B. Second-Order Processes

### 1. Spontaneous Emission in the Angular Momentum Basis

In [10], two-polariton spontaneous emission rates for  $s \rightarrow s$  transitions are computed. We now establish the formalism for the spontaneous emission of two vortices, thus opening up a path for analyzing the quantum optics of polaritons beyond first-order processes. The differential spontaneous emission into vortices at frequencies  $\omega_q$  and  $\omega_{q'}$  with wavevectors  $q$  and  $q'$  and angular momenta  $m$  and  $m'$  is [19]:

$$\Gamma = \frac{2\pi}{\hbar^2} \left( \frac{1}{2} \frac{L^2}{\pi^2} \int dq \int dq' \sum_{m,m'} \right) \left| \sum_{i_1} \frac{e\phi_{g,i_1} e\phi_{i_1,e}}{E_e - E_{i_1} + i0^+} \right|^2 \delta(\omega_0 - \omega_q - \omega_{q'}). \quad (32)$$

which inserting our potential operator (Equation (16)) yields:

$$\begin{aligned} \frac{d\Gamma}{d\omega}(e, 0 \rightarrow g, qm, q'm') &= \frac{1}{4}\pi\alpha^2 \frac{c^2}{v_g(\omega)v_g(\omega_0 - \omega)} \frac{\omega(\omega_0 - \omega)}{\bar{\epsilon}_r^2 \xi_q(\omega)\xi_{q'}(\omega_0 - \omega')} \times \\ &\left| \sum_n \frac{\langle g, qm, q'm' | J_{m'} e^{-im'\phi}(q'\rho) Z_{q'}(z) | n, qm \rangle \langle n, qm | J_m(q\rho) e^{-im\phi} Z_q(z) | e, 0 \rangle}{\omega_e - \omega_n - \omega_q} \right. \\ &\quad \left. + \frac{\langle g, qm, q'm' | J_m(q\rho) e^{-im\phi} Z_q(z) | n, q'm' \rangle \langle n, q'm' | J_{m'}(q'\rho) e^{-im'\phi} Z_{q'}(z) | e, 0 \rangle}{\omega_e - \omega_n - \omega_{q'}} \right|^2. \end{aligned} \quad (33)$$

For an  $s \rightarrow s$  transition in the long-wavelength approximation,  $\delta\ell = 1$  for each virtual transition, meaning that the virtual states can only have  $m = 0$  or  $m = \pm 1$ . The total differential decay rate is thus

$$\begin{aligned} \frac{d\Gamma}{d\omega}(e, 0 \rightarrow g, qq') &\equiv \sum_m \frac{d\Gamma}{d\omega}(e, 0 \rightarrow g, qm, q'(-m)) = \\ &\frac{d\Gamma}{d\omega}(e, 0 \rightarrow g, q0, q'0) + \frac{d\Gamma}{d\omega}(e, 0 \rightarrow g, q1, q'(-1)) + \frac{d\Gamma}{d\omega}(e, 0 \rightarrow g, q(-1), q'1) = \\ &\frac{d\Gamma}{d\omega}(e, 0 \rightarrow g, q0, q'0) + 2\frac{d\Gamma}{d\omega}(e, 0 \rightarrow g, q1, q' - 1). \end{aligned} \quad (34)$$

Using the fact that the matrix elements for the  $|m| = 1$  virtual transitions is  $\sqrt{2}$  smaller than that for the  $m = 0$  virtual transitions (see end of Sec. 4.1.1), the total decay rate is:

$$\frac{d\Gamma}{d\omega}(e, 0 \rightarrow g, qq') \equiv \sum_m \frac{d\Gamma}{d\omega}(e, 0 \rightarrow g, qm, q'(-m)) = \frac{3}{2} \frac{d\Gamma}{d\omega}(e, 0 \rightarrow g, q0, q'0) \quad (35)$$

Within the dipole approximation, the main contribution to the matrix elements in the sum over intermediate states comes from the  $zJ_0(0)\frac{dZ}{dz}\Big|_{z=z_0} = zZ'(z_0)$  term of the Taylor expansion of the field mode. Taking the emitter to be in the air region with  $Z = e^{-qz_0}$ , and defining  $\eta(\omega) \equiv \frac{q(\omega)c}{\omega}$ , we see that the differential decay rate is:

$$\begin{aligned} &\frac{3\pi\alpha^2}{8c^4\bar{\epsilon}_r^2} \left( \frac{1}{\xi_q(\omega)} \frac{c}{v_g(\omega)} \eta^2(\omega) e^{-2\eta(\omega)k(\omega)z_0} \right) \left( \frac{1}{\xi_{q'}(\omega_0 - \omega)} \frac{c}{v_g(\omega_0 - \omega)} \eta^2(\omega_0 - \omega) e^{-2\eta(\omega_0 - \omega)k(\omega_0 - \omega)z_0} \right) \times \\ &\omega^3(\omega_0 - \omega)^3 \left| z_{gn} z_{ne} \left( \frac{1}{\omega_e - \omega_n + \omega - \omega_0} + \frac{1}{\omega_e - \omega_n - \omega} \right) \right|^2, \end{aligned} \quad (36)$$

where  $z_{ab} \equiv \langle a | z | b \rangle$ . The two-photon differential emission rate in free-space, by comparison is [14]

$$\frac{d\Gamma}{d\omega}\Big|_{free\ space} = \frac{4}{3\pi c^4} \alpha^2 \omega^3 (\omega_0 - \omega)^3 \left| \sum_n z_{gn} z_{ne} \left( \frac{1}{\omega_e - \omega_n + \omega - \omega_0} + \frac{1}{\omega_e - \omega_n - \omega} \right) \right|^2.$$

$$\frac{d\Gamma/d\omega|_{\text{polaritons}}}{d\Gamma/d\omega|_{\text{free space}}} = \frac{9\pi^2}{32\epsilon_r^2} \left( \frac{1}{\xi_q(\omega)} \frac{c}{v_g(\omega)} \eta^2(\omega) e^{-2\eta(\omega)k(\omega)z_0} \right) \left( \frac{1}{\xi_q(\omega_0 - \omega)} \frac{c}{v_g(\omega_0 - \omega)} \eta^2(\omega_0 - \omega) e^{-2\eta(\omega_0 - \omega)k(\omega_0 - \omega)z_0} \right). \quad (37)$$

This result applies in the lossless limit of any highly confined polaritonic mode. All one needs is their  $\xi_q$  factors and their group velocities, which will be of order  $c/\eta$ . In order to check the validity of our result, we take the special case of a 2D plasmonic material. For graphene in the Drude model,  $c/v_g = 2\eta$  and  $\xi_q = 1$ , meaning that the two-photon enhancement in the angular momentum basis is  $\frac{9\pi^2}{8\epsilon_r^2} \eta^3(\omega) \eta^3(\omega_0 - \omega) \exp[-2\frac{z_0}{c}(\omega\eta(\omega) + (\omega_0 - \omega)\eta(\omega_0 - \omega))]$ , in agreement with the result in [10].

## 2. Absorption of Two-Vortices

The calculation of absorption of two vortices will be quite parallel to the calculation for emission except that factors of photon occupation number will be present. Therefore, in the lossless limit, the differential rate of two-vortex absorption is (assuming only  $m = 0$  vortices are present):

$$\frac{d\Gamma}{d\omega}(e, 0 \rightarrow g, q, q') = \frac{d\Gamma}{d\omega}(e, 0 \rightarrow g, q0, q'0) n_0(\omega) n_0(\omega_0 - \omega), \quad (38)$$

where  $n_0$  is the number of photons with zero angular momentum. The photon number is calculated in the same manner as detailed in the section on first-order transitions. The selection rule is of course that  $\Delta m = 0$ . More generally, the selection rule for an absorption transition involving two vortices of angular momenta  $m_1$  and  $m_2$  is that  $\Delta m = m_1 + m_2$ .

- 
- [1] M. Jablan, H. Buljan, and M. Soljačić, “Plasmonics in graphene at infrared frequencies,” *Physical review B*, vol. 80, no. 24, p. 245435, 2009.
  - [2] “*NIST Digital Library of Mathematical Functions*.” <http://dlmf.nist.gov/>, Release 1.0.13 of 2016-09-16. F. W. J. Olver, A. B. Olde Daalhuis, D. W. Lozier, B. I. Schneider, R. F. Boisvert, C. W. Clark, B. R. Miller and B. V. Saunders, eds.
  - [3] R. J. Glauber and M. Lewenstein, “Quantum optics of dielectric media,” *Physical Review A*, vol. 43, pp. 467–491, jan 1991.

- [4] S. Dai, Z. Fei, Q. Ma, A. Rodin, M. Wagner, A. McLeod, M. Liu, W. Gannett, W. Regan, K. Watanabe, *et al.*, “Tunable phonon polaritons in atomically thin van der waals crystals of boron nitride,” *Science*, vol. 343, no. 6175, pp. 1125–1129, 2014.
- [5] J. D. Caldwell, O. J. Glembocki, Y. Francescato, N. Sharac, V. Giannini, F. J. Bezares, J. P. Long, J. C. Owrutsky, I. Vurgaftman, J. G. Tischler, *et al.*, “Low-loss, extreme subdiffraction photon confinement via silicon carbide localized surface phonon polariton resonators,” *Nano letters*, vol. 13, no. 8, pp. 3690–3697, 2013.
- [6] P. Alonso-Gonzalez, A. Y. Nikitin, Y. Gao, A. Woessner, M. B. Lundberg, A. Principi, N. Forcellini, W. Yan, S. Velez, A. Huber, *et al.*, “Ultra-confined acoustic thz graphene plasmons revealed by photocurrent nanoscopy,” *arXiv preprint arXiv:1601.05753*, 2016.
- [7] V. D. Karanikolas, C. A. Marocico, P. R. Eastham, and A. L. Bradley, “Near-field relaxation of a quantum emitter to 2d semiconductors: surface dissipation and exciton polaritons,” *arXiv preprint arXiv:1608.02747*, 2016.
- [8] P. Li, X. Yang, T. W. Maß, J. Hanss, M. Lewin, A.-K. U. Michel, M. Wuttig, and T. Taubner, “Reversible optical switching of highly confined phonon-polaritons with an ultrathin phase-change material,” *Nature materials*, 2016.
- [9] T. Low, R. Roldán, H. Wang, F. Xia, P. Avouris, L. M. Moreno, and F. Guinea, “Plasmons and screening in monolayer and multilayer black phosphorus,” *Physical review letters*, vol. 113, no. 10, p. 106802, 2014.
- [10] N. Rivera, I. Kaminer, B. Zhen, J. D. Joannopoulos, and M. Soljačić, “Shrinking light to allow forbidden transitions on the atomic scale,” *Science (New York, N.Y.)*, vol. 353, pp. 263–9, jul 2016.
- [11] D. P. Craig and T. Thirunamachandran, *Molecular quantum electrodynamics: an introduction to radiation-molecule interactions*. Courier Corporation, 1984.
- [12] D. Guéry-Odelin and C. Cohen-Tannoudji, *Advances in Atomic Physics*. World Scientific, 2011.
- [13] F. H. Koppens, D. E. Chang, and F. J. Garcia de Abajo, “Graphene plasmonics: a platform for strong light–matter interactions,” *Nano letters*, vol. 11, no. 8, pp. 3370–3377, 2011.
- [14] G. Breit and E. Teller, “Metastability of hydrogen and helium levels,” *The Astrophysical Journal*, vol. 91, p. 215, 1940.
- [15] Note that this does *not* mean that we have already switched from the  $\phi = 0$  gauge to the Coulomb gauge, where the vector potential is approximately zero. We merely mean that the mathematical form

of the electric field or vector potential modes in the  $\phi = 0$  gauge is the gradient of a scalar function (i.e., the field is approximately curl-free). This is the real-space definition of field longitudinality. In general, a purely longitudinal field can indeed be represented by having zero scalar potential and a non-zero but longitudinal vector potential.

- [16] The calculation scheme follows the treatments described in [11, 12] In this scheme, the initial state is taken such that the initial state of the electromagnetic field represents a collection of photons in a continuum of modes  $\{q\}$  with respective photon number  $\{n(q)\}$ . The continuum of final states arises from all of the ways that one photon can be removed from this distribution. The delta function in Fermi's Golden Rule picks "the number of photons" at the frequency of interest. For a more complicated initial state representing a superposition of photon number distributions, the mean number of photons at the frequency of interest shows up instead. We put this in quotes because it is impossible to have a finite number of photons in each mode if the modes form a continuum. Such a state would have clearly infinite energy. However it is possible to define the photon number in a way that is in agreement with the treatment in which a semi-classical treatment of the field is used. We do so in what follows.
- [17] It is also worth noting that when the field contains many photons and can be treated semiclassically, the absorption rate can be shown to be the same as what we derive here given that we define photon number in the way shown above. The answer one would get by applying first-order time-dependent perturbation theory is  $\Gamma = \frac{2\pi e^2}{\epsilon_0 m^2 \omega_0^2 \hbar^2} \int d\mathbf{r} d\mathbf{r}' \left( \frac{d\langle u_{ij} \rangle}{d\omega} \Big|_{\omega_0} (\mathbf{r}, \mathbf{r}') \right) \psi_f^*(\mathbf{r}) \psi_f(\mathbf{r}') p_i p_j^* \psi_i(\mathbf{r}) \psi_i^*(\mathbf{r}')$ , where  $\left( \frac{d\langle u_{ij} \rangle}{d\omega} \Big|_{\omega_0} (\mathbf{r}, \mathbf{r}') \right)$  is the time-averaged cross-spectral density evaluated at two space points. The time-averaged cross-spectral density is simply the time-average of  $\epsilon_0 E_i(\mathbf{r}, \omega) E_j^*(\mathbf{r}', \omega)$ , where  $E_i(\mathbf{r}, \omega)$  is the Fourier transform of the  $i$ -th component of the semiclassical electric field. This can be seen as a generalization of Einstein's theory of absorption in which the absorption rate is proportional to the power spectral density at the location of the atom. The power spectral density is the trace of the time-averaged cross-spectral density evaluated at the same space points. For non-dipole transitions, the dependence on energy density is more complicated as a result of the spatial extent of the electronic wavefunctions.
- [18] We do not need to change the unperturbed wavefunctions due to a theorem which states that transition amplitudes computed between states of the same energy are the same using the same unperturbed states in any gauge [11].

[19] Note that strictly speaking, we're ignoring the effect intermediate levels in-between the initial and final states. We can assume there aren't any or realize that the effect of them is to create a radiative cascade which is effectively first-order in perturbation theory. To optimize two-photon spontaneous emission, one would want to suppress or avoid radiative cascades as much as possible. It is described how to do so in [10]. For absorption, one simply wants to avoid exciting at frequencies that would resonantly excite a state in-between the initial and final states.